Change in Frozen Soils and Its Effect on Regional Hydrology in the Upper Heihe Basin, on the Northeastern Qinghai-Tibetan Plateau

Bing Gao[1], Dawen Yang[2]*, Yue Qin[2], Yuhan Wang[2], Hongyi Li[3], Yanlin Zhang[3], and Tingjun Zhang[4]

[1] School of Water Resources and Environment, China University of Geosciences, Beijing 100083, China

[2] State Key Laboratory of Hydroscience and Engineering, Department of Hydraulic Engineering, Tsinghua University, Beijing 100084, China

[3] Cold and Arid Regions Environmental and Engineering Research Institute, Chinese Academy of Sciences, Lanzhou, Gansu 730000, China

[4] Key Laboratory of West China's Environmental Systems (MOE), College of Earth and Environmental Sciences, Lanzhou University, Lanzhou, 730000, China

* *Correspondence to*: Dawen Yang (yangdw@tsinghua.edu.cn)

To be submitted to: The Cryosphere, August, 2017

ABSTRACT:

Frozen ground has an important role in regional hydrological cycles and ecosystems, especially on the Qinghai-Tibetan Plateau, which is characterized by high elevation and a dry climate. This study modified a distributed physically based hydrological model and applied it to simulate the long-term (from 1971 to 2013) change of frozen ground and its effect on hydrology in the upper Heihe basin located in the northeastern Qinghai-Tibetan Plateau. The model was validated carefully against data obtained from multiple ground-based observations. Based on the model simulations, we analyzed the changes of frozen soils and their effects on the hydrology. The results showed that the permafrost area shrank by 9.5% (approximately 600 km^2), especially in areas with elevation between 3500 m and 3900 m. The maximum frozen depth of seasonally frozen ground decreased at a rate of approximately 5.2 cm/10yr, and the active layer thickness over the permafrost increased by about 3.5 cm/10yr. Runoff increased significantly during cold seasons (November-March) due to the increase in liquid soil moisture caused by rising soil temperature. Areas where permafrost changed into seasonally frozen ground at high elevation showed especially large increase in runoff. Annual runoff increased due to increased precipitation, the base flow increased due to permafrost degradation, and the actual evapotranspiration increased significantly due to increased precipitation and soil warming. The groundwater storage showed an increasing trend, which indicated that the groundwater recharge was enhanced mainly due to the degradation of permafrost in the study area.

KEYWORDS: permafrost; seasonally frozen ground; soil moisture; soil temperature;

runoff

1. Introduction

Global warming has led to significant changes in frozen soils, including both permafrost and seasonally frozen ground at high latitudes and high altitudes (Hinzman et al., 2013; Cheng and Wu, 2007). Changes in frozen soils can greatly affect the land-atmosphere interaction and the energy and water balances of the land surface (Subin et al., 2013; Schuur et al., 2015), altering soil moisture, water flow pathways and stream flow regimes (Walvoord and Kurylyk, 2016). Understanding the changes in frozen soils and their impact on regional hydrology is important for water resources management and ecosystem protection in cold regions.

Previous studies based on either experimental observations or long-term meteorological or hydrological observations have examined changes in frozen soils and their impacts on hydrology. Several studies reported that permafrost thawing might enhance base flow in the Arctic and the Subarctic (Walvoord and Striegl, 2007; Jacques and Sauchyn, 2009; Ye et al., 2009) and in northeast China (Liu et al., 2003; Duan et al., 2017). A few studies reported that permafrost thawing might reduce river runoff (This paper defines the runoff as all liquid water flowing out of the study area.), especially in the Qinghai-Tibetan Plateau (e.g. Qiu, 2012; Jin et al., 2009). Intensive field observations were usually carried out at small spatial scales over short periods, which lacked the regional pattern and long-term trends of the frozen soils. And the long-term meteorological and hydrological observations did not provide detailed data on soil freezing and thawing processes (McClelland et al., 2004; Liu et al., 2003; Niu et al., 2011). Therefore, previous observation-based studies have not provided a sufficient

64 understanding of the long-term changes in frozen soils and their impact on regional
65 hydrology (Woo et al., 2008).

66 Hydrological models have been coupled with soil freezing-thawing schemes to
67 simulate impacts of the changes in frozen soils on catchment hydrology. Several
68 hydrological models (Rawlins et al., 2003; Chen et al., 2008) used simple freezing-
69 thawing schemes, which could not simulate the vertical soil temperature profiles. The
70 SiB2 model (Sellers et al., 1996), the modified VIC model (Cherkauer and Lettenmaier,
71 1999) and the CLM model (Oleson et al., 2010) simulate vertical soil freezing-thawing
72 processes, but they represent the flow routing at the catchment scale by simplified ways.
73 Subin et al. (2013) and Lawrence et al. (2015) used the CLM model to simulate the
74 global change of permafrost. Cuo et al. (2015) used the VIC to simulate frozen soil
75 degradation and its hydrological impacts at the plot scale in the headwater of the Yellow
76 River. The GEOtop model (Endrizzi et al., 2014) simulates three-dimensional water
77 flux and vertical heat transfer in soil, but it is difficult to apply to regional scales. Wang
78 et al. (2010) and Zhang et al. (2013) incorporated frozen soil schemes in a distributed
79 hydrological model and showed improved performance in a small mountainous
80 catchment. More regional studies are necessary for better understanding of the frozen
81 soil changes and their impacts on the regional hydrology and water resources.

82 The Qinghai-Tibetan Plateau is known as Asia's water tower, and runoff changes
83 on the plateau have significant impacts on water security in downstream regions (Walter
84 et al., 2010), which have received an increasing amount of attention in recent years
85 (Cuo et al., 2014). The Qinghai-Tibetan Plateau is characterized by high elevation and

cold climate. Cryospheric processes have great impacts on its hydrological processes (Cheng and Jin, 2013; Cuo et al., 2014). In contrast with the Arctic and Subarctic, the permafrost on the Qinghai-Tibetan Plateau is relatively thin and warm, and the frozen depth of the seasonally frozen soils is also relatively shallow. As a result, the frozen soils on the Qinghai-Tibetan Plateau are more sensitive to air temperature rising (Yang et al., 2010), and the changes of frozen soils may have more significant impacts on regional hydrology.

An evident increase in the annual and seasonal air temperature has been observed in the Qinghai-Tibetan Plateau (Li et al., 2005; Liu and Chen, 2000; Zhao et al., 2004). Several studies have shown the changes of frozen soils based on long-term observations. For example, Cheng and Wu (2007) analyzed the borehole observations of soil temperature profiles on the Qinghai-Tibetan Plateau and found that the active layer thickness of frozen soils increased by 0.15-0.50 m during the period of 1996-2001. Zhao et al. (2004) found a decreasing trend of freezing depth in the seasonally frozen soils using observations at 50 stations. Several studies have analyzed the relationship between the change of frozen soils and river discharge using the observed data (Zhang et al., 2003; Jin et al., 2009; Niu et al., 2011). However, the spatio-temporal characteristics of the long-term change in frozen soils are not sufficiently clear. Based on comprehensive field experiments (Cheng et al., 2014), a hydrological model coupling cryospheric processes and hydrological processes has been developed (Gao et al., 2016). This provides a solid basis upon which to analyze the spatio-temporal changes in frozen soils and their impacts on the regional hydrology in the upper Heihe

basin located on the northeastern Qinghai-Tibetan Plateau.

On the basis of the previous studies, this study aims to: (1) explore the spatial and temporal changes of frozen soils using a distributed hydrological model with comprehensive validation and (2) analyze the hydrological responses to the change of frozen soils during the past 40 years in the upper Heihe basin.

2. Study Area and Data

The Heihe River is one of the major inland basins in northwestern China. As shown in Figure 1, the upper reaches of the Heihe River are located on the northeastern Qinghai-Tibetan Plateau at an elevation of 2200 to 5000 m with a drainage area of 10,009 km^2. The upper reaches provide the majority of the water supplied to the middle and lower reaches (Cheng et al., 2014). The annual precipitation in the upper Heihe basin ranges from 200 to 700 mm, and the mean annual air temperature ranges from -9 to 5℃. Permafrost dominates the high elevation region above 3700 m (Wang et al., 2013), and seasonal frozen ground covers other parts of the study area. Glaciers are found at an elevation above 4000 m, covering approximately 0.8% of the upper Heihe basin. There are two tributaries (East and West Tributaries) in the upper Heihe basin, on which two hydrological stations are located, namely, Qilian (on the east tributary) and Zhamashike (on the west tributary). The outlet of the upper Heihe basin has a hydrological station, namely, Yingluoxia (see Figure 1).

The spatial data used in this study includes the atmospheric forcing data, the land surface data and the actual evapotranspiration data based on remote sensing. The atmospheric forcing data include a 1-km gridded dataset of daily precipitation, air

temperature, sunshine hours, wind speed and relative humidity. The gridded daily precipitation was interpolated from observations at meteorological stations (see Figure 1) using the method developed by Wang et al. (2017) provided by the China Meteorological Administration (CMA). The other atmospheric forcing data were interpolated by observations at meteorological stations using the inverse distance weighted method. The interpolation of air temperature considers the temperature gradient with elevation which was provided by the HiWATER experiment (Li et al., 2013).

The land surface data used to run the model include land use, topography, leaf area index, and soil parameters. The topography data were obtained from the SRTM dataset (Jarvis et al., 2008) with a spatial resolution of 90 m. The land use/cover data were provided by the Institute of Botany, Chinese Academy of Sciences (Zhou and Zheng, 2014). The leaf area index (LAI) data with 1-km resolution were developed by Fan (2014). The soil parameters were developed by Song et al. (2016); they include the saturated hydraulic conductivity, residual soil moisture content, saturated soil moisture content, soil sand matter content, soil clay matter content and soil organic matter content. Monthly actual evapotranspiration data with 1-km resolution during the period of 2002-2012 estimated based on remote sensing data (Wu et al., 2012; Wu, 2013).

Field observation data used in this study includes river discharge, soil temperature, frozen depth, soil moisture and borehole observation. Daily river discharge data were obtained from the Hydrology and Water Resources Bureau of Gansu Province. Daily soil temperature data collected at the Qilian station from January 1, 2004 to December

31, 2013, and daily frozen depth data collected at the Qilian and Yeniugou stations from January 1, 2002 to December 31, 2013 were provided by CMA.

Temperature observations from six boreholes, whose location are shown in Figure 1, were provided by Wang et al. (2013). The borehole depths are 100 m for T1, 69 m for T2, 50 m for T3, 90 m for T4, and 20 m for T5 and T7. The HiWATER experiment (Li et al., 2013; Liu et al., 2011) provided the soil moisture data from January 1 to December 31, 2014 at the A'rou Sunny Slope station (100.52 E, 38.09 N).

3. Methodology

3.1 Brief introduction of the hydrological model

This study used a distributed eco-hydrological model GBEHM (geomorphology-based ecohydrological model), which was developed by Yang et al. (2015) and Gao et al. (2016) based on the geomorphology-based hydrological model (Yang et al., 1998 and 2002; Cong et al., 2009). GBEHM is a spatial distributed model for large-scale river basin. It employs the geomorphologic properties to reduce the lateral two-dimensions into one-dimension for flow routing within a sub-catchment, which greatly improves the computation efficiency while retaining the spatial heterogeneity in water flow paths at basin scale. As shown in Figure 2, the GBEHM used a 1-km grid system to discretize the study catchment, and the study catchment was divided into 251 sub-catchments. A sub-catchment was further divided into flow-intervals along its main stream. To capture the sub-grid topography, each 1-km grid was represented by a number of hillslopes with an average length and gradient, but different aspect, which were estimated from the 90-m DEM. The terrain properties of a hillslope include the slope length and gradient,

slope aspect, soil type and vegetation type (Yang et al., 2015).

The hillslope is the basic unit for the hydrological simulation, upon which the water and heat transfers (both conduction and convection) in the vegetation canopy, snow/glacier, and soil layers are simulated. The canopy interception, radiation transfer in the canopy and the energy balance of the land surface are described using the methods of SIB2 (Sellers et al., 1985, 1996). The surface runoff on the hillslope is solved using the kinematic wave equation. The groundwater aquifer is considered as individual storage units corresponding to each grid. Exchange between the groundwater and the river water is calculated using Darcy's law (Yang et al., 1998, 2002).

The model runs with a time step of 1 hour. Runoff generated from the grid is the lateral inflow into the river at the same flow interval in the corresponding sub-catchment. Flow routing in the river network is calculated using the kinematic wave equation following the sequence determined by the Horton-Strahler scheme (Strahler, 1957). The model is driven by the atmosphere forcing data and land surface data which are introduced in section 2.

3.2 Simulation of cryospheric processes

The simulation of cryospheric processes in GBEHM includes glacier ablation, snow melt, and soil freezing and thawing.

(1) Glacier ablation

Glacier ablation is simulated using an energy balance model (Oerlemans, 2001) as:

$$Q_M = SW(1-\alpha) + LW_{in} - LW_{out} - Q_H - Q_L - Q_G + Q_R \quad (1)$$

where Q_M is the net energy absorbed by the surface of the glacier (W/m^2); SW is the

196 incoming shortwave radiation (W/m^2); α is the surface albedo; LW_{in} is the incoming
197 longwave radiation (W/m^2); LW_{out} is the outgoing longwave radiation (W/m^2); Q_H is
198 the sensible heat flux (W/m^2); Q_L is the latent heat flux (W/m^2); Q_R is the energy from
199 rainfall (W/m^2); and Q_G is the penetrating shortwave radiation (W/m^2). The surface
200 albedo is calculated as (Oerlemans and Knap, 1998):

201 $$\alpha = \alpha_{snow} + (\alpha_{ice} - \alpha_{snow}) e^{-h/d^*} \quad (2)$$

202 where α_{snow} is the albedo of snow on the glacier surface; α_{ice} is the albedo of the ice
203 surface; h is the snow depth on the glacier surface (m); d^* is a parameter of the snow
204 depth effect on the albedo (m).

205 The amount of melt water is calculated as (Oerlemans, 2001):

206 $$M = \frac{Q_M}{L_f} dt \quad (3)$$

207 where dt is the time step used in the model (s) and L_f is the latent heat of fusion (J/kg).

208 (2) Snow melt

209 A multi-layer snow cover model is used to describe the mass and energy balance of
210 snow cover. The parametrization of snow is based on Jordan (1991), and each snow
211 layer is described by two constituents, namely, ice and liquid water. For each snow layer,
212 temperature is solved using an energy balance approach (Bartelt and Lehnin, 2002):

213 $$C_s \frac{\partial T_s}{\partial t} - L_f \frac{\partial \rho_i \theta_i}{\partial t} = \frac{\partial}{\partial z}(K_s \frac{\partial T}{\partial z}) + \frac{\partial I_R}{\partial z} + Q_R \quad (4)$$

214 where C_s is the heat capacity of snow (J·m^{-3}·K^{-1}); T_s is the temperature of the snow
215 layer (K); ρ_i is the density of the ice (kg/m^3); θ_i is the volumetric ice content;
216 K_s is the thermal conductivity of snow (W·m^{-1}·K^{-1}); L_f is the latent heat of ice fusion
217 (J/kg) ; I_R is the radiation transferred into the snow layer (W/m^2) and Q_R is the energy

brought by rainfall (W/m^2) which is only considered for the top snow layer. The solar radiation transfer in the snow layers and the snow albedo are simulated using the SNICAR model which is solved using the method developed by Toon et al. (1989). Eq. (4) is solved using an implicit centered finite difference method, and a Crank-Nicholson scheme is employed.

The mass balance of the snow layer is described as (Bartelt and Lehnin, 2002):

$$\frac{\partial \rho_i \theta_i}{\partial t} + M_{iv} + M_{il} = 0 \tag{5}$$

$$\frac{\partial \rho_l \theta_l}{\partial t} + \frac{\partial U_l}{\partial z} + M_{lv} - M_{il} = 0 \tag{6}$$

where ρ_l is the density of the liquid water (kg/m^3); θ_l is the volumetric liquid water content; U_l is the liquid water flux ($kg \cdot m^{-2} \cdot s^{-1}$); M_{iv} is the mass of ice that is changed into vapour within a time step ($kg \cdot m^{-3} \cdot s^{-1}$); M_{il} is the mass of ice that is changed into liquid water within a time step ($kg \cdot m^{-3} \cdot s^{-1}$); and M_{lv} is the mass of liquid water that is changed into vapour within a time step ($kg \cdot m^{-3} \cdot s^{-1}$). The liquid water flux of the snow layer is calculated as (Jordan, 1991):

$$U_l = -\frac{k}{\mu_l} \rho_l^2 g \tag{7}$$

where k is the hydraulic permeability (m^2), μ_l is dynamic viscosity of water at 0 ℃ (1.787×10^{-3} N s/m^2), ρ_l is the density of liquid water (kg/m^3) and g is gravitational acceleration (m/s^2). The water flux of the bottom snow layer is considered snowmelt runoff.

(3) Soil freezing and thawing

The energy balance of the soil layer is solved as (Flerchinger and Saxton, 1989):

$$C_s \frac{\partial T}{\partial t} - \rho_i L_f \frac{\partial \theta_i}{\partial t} - \frac{\partial}{\partial z}(\lambda_s \frac{\partial T}{\partial z}) + \rho_l c_l \frac{\partial q_l T}{\partial z} = 0 \quad (8)$$

where C_s is the volumetric soil heat capacity ($J \cdot m^{-3} \cdot K^{-1}$); T is the temperature (K) of the soil layers; z is the vertical depth of the soil (m); θ_i is the volumetric ice content; ρ_i is the density the ice (kg/m^3); λ_s is the thermal conductivity ($W \cdot m^{-1} \cdot K^{-1}$); ρ_l is the density of liquid water (kg/m^3); and c_l is the specific heat of liquid water ($J \cdot kg^{-1} \cdot K^{-1}$). In addition, q_l is the water flux between different soil layers (m/s) and is solved using the 1-D vertical Richards equation. The unsaturated soil hydraulic conductivity is calculated using the modified van Genuchten's equation (Wang et al., 2010) as:

$$K = f_{ice} K_{sat} (\frac{\theta_l - \theta_r}{\theta_s - \theta_r})^{1/2} [1 - (1 - (\frac{\theta_l - \theta_r}{\theta_s - \theta_r})^{-1/m})^m]^2 \quad (9)$$

where K is the unsaturated soil hydraulic conductivity (m/s); K_{sat} is the saturated soil hydraulic conductivity (m/s); θ_l is the volumetric liquid water content; θ_s is the saturated water content; θ_r is the residual water content; m is an empirical parameter in van Genuchten's equation and f_{ice} is an empirical hydraulic conductivity reduction factor which is calculated using soil temperature as (Wang et al., 2010):

$$f_{ice} = \exp[-10(T_f - T_{soil})], \quad 0.05 \le fice \le 1 \quad (10)$$

where T_f is 273.15 K and T_{soil} is the soil temperature.

Eq. (8) solves the soil temperature with the upper boundary condition as the heat flux into the top surface soil layer. When the ground is not covered by snow, the heat flux from the atmosphere into the top soil layer is expressed as (Oleson et al., 2010):

$$h = S_g + L_g - H_g - \lambda E_g + Q_R \quad (11)$$

where h is the upper boundary heat flux into the soil layer ($W\ m^{-2}$); S_g is the solar

261 radiation absorbed by the top soil layer (W m^{-2}); L_g is the net long wave radiation
262 absorbed by the ground (W m^{-2}), H_g is the sensible heat flux from the ground (W m^{-2});
263 λE_g is the latent heat flux from the ground (W m^{-2}); and Q_R is the energy brought by
264 rainfall (W/m^2). When the ground is covered by snow, the heat flux into the top soil
265 layer is calculated as:

266 $$h = I_p + G \tag{12}$$

267 where I_p is the radiation that penetrates the snow cover, and G is the heat conduction
268 from the bottom snow layer to the top soil layer. Eq (8) is solved using a finite difference
269 scheme with an hourly time step which is similar with the solutions of Eq (4).

270 To simulate the permafrost we consider an underground depth of 50 m. We assume
271 the bottom boundary condition as zero heat flux exchange due to the data limitation.
272 This assumption may not be true because the observed soil temperature increased with
273 depth in the deep layer. The vertical soil column is divided into 39 layers in the model
274 (see Figure 2). As shown in Figure 2, thinner layers are used at the depth from 1.7 to 3
275 m for better capturing the maximum frozen depth according to the field observations.
276 The topsoil of 1.7 m is subdivided into 9 layers. The first layer is 5 cm, and the soil
277 layer thickness increases with depth linearly from 5 cm to 30 cm up to the depths of 0.8
278 m and later decreases linearly with depth to 10 cm up to the depths of 1.7 m. There are
279 12 soil layers from 1.7 m to 3.0 m with a constant thickness of 10 cm. From the depth
280 of 3 m to 50 m, there are 18 layers with thickness increasing exponentially from 10 cm
281 to 12 m. The liquid soil moisture, ice content, and soil temperature of each layer is
282 calculated at each time step. The soil heat capacity and soil thermal conductivity are

283 estimated using the method developed by Farouki (1981).

284 **3.3 Model calibration**

285 To initialize the model, we first estimated the soil temperature profiles based on the
286 assumption that there is a linear relationship between soil temperature and elevation at
287 the same depth below surface. The relationship between soil temperature at a specific
288 depth and elevation is estimated from the observed soil temperature at 6 boreholes (see
289 Figure 1). Next, the model had a 500 year spin up run to specify the initial values of the
290 hydrological variables (e.g., soil moisture, soil temperature, soil ice content, and
291 groundwater table) by repeating the atmospheric forcing data from 1961 to 1970.

292 The period of 2002 to 2006 was used for model calibration and the period of 2008 to
293 2012 was for model validation. The daily soil temperature at the Qilian station and the
294 frozen depths at the Qilian and Yeniugou stations were used to calibrate the soil
295 reflectance according to vegetation type. The other parameters such as groundwater
296 hydraulic conductivity were calibrated according to the observed baseflow discharge in
297 the winter season at the Qilian, Zhamashike and Yingluoxia stations. We calibrated the
298 surface retention capacity and surface roughness to match the observed flood peaks,
299 and calibrated the leaf reflectance, leaf transmittance and maximum Rubsico capacity
300 of the top leaf based on the remote sensing evapotranspiration data. Table 1 shows the
301 major parameters used in the model.

302 **3.4 Simulation case without the frozen soil scheme**

303 A simulation case without the frozen soil scheme is designed to investigate the impact
304 of frozen soil on the hydrological processes. In this case, the phase transition of soil

305 water between the solid and the liquid is not considered although soil temperature is
306 still simulated. Other processes are simulated as the same as the normal run.

307 **4. Results**

308 **4.1 Validation of the hydrological model**

309 We carried out a comprehensive validation of the GBEHM model using the soil
310 temperature profiles observed at six boreholes, long-term observations of the soil
311 temperature and frozen depths at the Qilian and Zhamashike stations, soil moisture
312 observations at the A'rou Sunny Slope station, long-term observations of streamflow at
313 three hydrological stations shown in Figure 1 and monthly actual evapotranspiration
314 estimated from remote sensing data.

315 Figure 3 shows the comparison of the model-simulated and observed soil
316 temperature profiles at six boreholes. The model generally captured the vertical
317 distribution of the soil temperature at T1, T2, T3 and T4 in the permafrost area, but
318 overestimations were produced above 20 m depth for T1 and T3. Good agreement
319 between the simulated and observed soil temperature profiles below the depth of 20 m
320 is probably due to fitting of initial values. This implies that the temperature in the deep
321 soil is stable, which is confirmed by the comparison of temperature profiles in different
322 years as shown in Figure S1 in the supplemental file. Figure S1 also illustrates that
323 temperature above 20 m shows significant increasing trends in the past 40 years. The
324 errors in simulating the vertical temperature profile near the surface might be caused
325 by simplification of the 3-D topography. At T5 located in seasonally frozen ground, the
326 simulated soil temperature profile did not agree well with that observed at depth of 4-

20 m. This error might also be related to the heterogeneity of soil properties, especially the thermal conductivity and heat capacity since no such information is available. The model simulation agrees well with the borehole observation at T7, which is located at the transition zone from permafrost to seasonally frozen ground. This indicates that the model can identify the boundary of the permafrost and the seasonally frozen ground.

We also validated model simulation of the freezing/thawing cycles based on long-term observations of soil temperature and frozen depth. Figure 4 compares the simulated soil temperature with the observed temperature at the Qilian station, which is located in the seasonally frozen ground (observed daily soil temperature data are available from 2004 on). Generally, the model simulations accurately captured the seasonal changes in soil temperature profile. Validation of the soil temperature at different depths (5 cm, 10 cm, 20 cm, 40 cm, 80 cm, 160 cm, and 320 cm) showed that the root mean square error (RMSE) decreases with increasing depth. The RMSE were approximately 2.5℃ for the top three depths (5 cm, 10 cm and 20 cm). The RMSE for depths of 40 cm and 80 cm were 1.7℃ and 1.5℃, respectively, and the RMSE was 0.9℃ at a depth of 3.2 m. This result is similar with the findings by Ou et al. (2016) using the Northern Ecosystem Soil Temperature (NEST) model. We compared the model-simulated daily frozen depth with in situ observations at the Qilian and Yeniugou Stations from 2002 to 2014, as shown in Figure 5. The model reproduced well the daily variations in frozen depth although the depth was underestimated by approximately 50 cm at the Yeniugou station. In general, the validation of soil temperature and frozen depth indicates that the model captured well the freezing and thawing processes in the

upper Heihe basin.

The observed hourly liquid soil moisture at the A'rou Sunny Slope station was used for an additional independent validation. Figure 6 shows the comparison between the simulated and observed liquid soil moisture at different depths from January 1 to December 31 in 2014. By comparing with the observed liquid soil moisture, we can see that the model simulation is reasonable.

Figure 7 compares the model simulated and the observed daily streamflow discharge at the Yingluoxia, Qilian and Zhamashike stations. The model simulation agreed well with the observations. The model simulation captured the flood peaks and the magnitude of base flow in both of the calibration and validation periods. In the calibration period, the Nash-Sutcliffe efficiency (NSE) coefficients were 0.64, 0.65 and 0.70 for the Yingluoxia, Qilian and Zhamashike stations, respectively; in the validation period, the NSE values were 0.65, 0.60, and 0.75, respectively. The relative error (RE) was within 10% for both the calibration and validation periods (see Figure 7). Figure 8 shows the comparison of the model-simulated monthly actual evaporation and remote sensing-based evaporation data for the entire calibration and validation periods. The GBEHM simulation showed similar temporal variations in actual evapotranspiration compared with the remote sensing based estimation, and the RMSE of the simulated monthly evapotranspiration was 8.0 mm in the calibration period and 6.3 mm in the validation period.

The model simulated river discharges with and without the frozen soil scheme were compared. Table S1 in the supplement material shows that model with the frozen soil

scheme achieves better simulation of the daily hydrograph than the model without the frozen soil scheme. Figure S2 in the supplement material shows that the model without the frozen soil scheme overestimated the river discharge in the freezing season and underestimated flood peaks in the warming season.

4.2 Long-term changes in frozen soils

In the upper Heihe basin, the ground surface starts freezing in November and thawing initiates in April (Wang et al., 2015a). From November to March, the ground surface temperature is below 0℃ in both the permafrost and seasonally frozen ground regions, and precipitation mainly falls in the period from April to October. Therefore, a year is subdivided into two seasons, i.e., the freezing season (November to March) and the thawing season (April to October) to investigate the changes in frozen soils and their hydrological impact. Increasing precipitation and air temperature in the study area in both seasons in the past 50 years was reported in a previous study (Wang et al., 2015b). Table S2 in the supplement material shows that annual mean air temperature increased by approximately 1.2℃ in the period of 2001 to 2010 comparing with the period of 1971 to 1980. And air temperature in the freezing season shows larger increase (approximately 1.4℃) than in the thawing season(1.1℃) between these two periods.

Figure 9 shows the changes in the basin-averaged soil temperature in the freezing and thawing seasons. The soil temperature increased in all seasons, especially in the past 30 years. The increasing trend of soil temperature was larger in the freezing season than in the thawing season. In the freezing season (Figure 9(a)), the top layer soil temperature was lower than the deep layer soil temperature. The linear trend of the top

layer (0-0.5 m) soil temperature was 0.48℃/10yr and the trend of the deep layer (2.5-3 m) soil temperature was 0.34℃/10yr. The soil temperature in the deep layer (2.5-3 m) changed from -1.1℃ in the 1970s to approximately 0℃ in the most recent decade. In the thawing season (see Figure 9(b)), the increasing trend of the top layer (0-0.5 m) soil temperature (0.29℃/10yr) was greater than the trend of the deep layer (2.5-3 m) soil temperature (0.21℃/10yr). The warming trend is larger in shallow soils and this is because the surface heat flux is impeded by the thermal inertia as it penetrates to greater depths.

Permafrost is defined as ground with a temperature at or below 0℃ for at least two consecutive years (Woo, 2012). This study differentiated permafrost from seasonally frozen ground based on the simulated vertical soil temperature profile in each grid. For each year in each grid, the frozen ground condition was determined by searching the soil temperature profile within a four-year window from the previous three years to the current year. Figure 10 shows the change in permafrost area during 1971-2013. As shown in Figure 10(a), the permafrost areas decreased by approximately 9.5% (from 6445 km^2 in the 1970s to 5831 km^2 in the 2000s), indicating evident degradation of the permafrost in the upper Heihe basin in the past 40 years.

Figure 10 (b) shows the changes in the basin-averaged maximum frozen depth for the seasonally frozen ground areas and active layer thickness over the permafrost areas. The basin-averaged annual maximum frozen depth showed a significant decreasing trend (5.2 cm/10yr). In addition, the maximum frozen depth had a significantly negative correlation with the annual mean air temperature (r = -0.73). An increasing trend of

active layer thickness in the permafrost regions was observed (3.5 cm/10yr), which had a significantly positive correlation with the annual mean air temperature.

Figure 11 shows the frozen soil distributions in the period of 1971 to 1980 and in the period of 2001 to 2010. Comparing the frozen soil distributions of the two periods, major changes in frozen soils were observed on the sunny slopes at elevations between 3500 and 3700 m, especially in the west tributary, where large areas of permafrost changed into seasonally frozen ground.

Figure 12 shows the monthly mean soil temperature over the areas with elevation between 3300 and 3500 m and over areas with elevation between 3500 and 3700 m in the upper Heihe basin. In the areas with elevation between 3300 and 3500 m located in the seasonally frozen ground region, as shown in Figure 12(a), the frozen depth decreased and the soil temperature in the deep layer (with depth greater than 2 m) increased. Figure 12(b) shows that the increase in soil temperature was larger in the area with higher elevation (3500-3700 m). This figure shows that the thickness of the permafrost layer decreased as soil temperature increased, and the permafrost changed into seasonally frozen ground after 2000.

4.3 Changes in the water balance and runoff

Table 2 shows the decadal changes in the annual water balance from 1971 to 2010 based on the model simulation. The annual precipitation, annual runoff and annual runoff ratio had the same decadal variation; however the annual evapotranspiration maintained an increasing trend since the 1970s which was consistent with the rising air temperature and soil warming. Although the actual evapotranspiration increased, the

runoff ratio remained stable during the 4 decades because of the increased precipitation.

The changes in runoff (both simulated and observed) in different seasons are shown in Figure 13 and Table 2. The model-simulated and observed runoff both showed a significant increasing trend in the freezing season and in the thawing season. This indicates that the model simulation well reproduced the observed long-term changes. In the freezing season, since there was no glacier melt and snow melt (see Table 2), runoff was mainly the subsurface flow (groundwater flow and lateral flow from the unsaturated zone). In the thawing season, as shown in Table 2, snowmelt runoff contributed approximately 16% of the total runoff and glacier runoff contributed only a small fraction of total runoff (approximately 2.4%). Therefore, rainfall runoff was the major component of total runoff in the thawing season, and the runoff increase in the thawing season was mainly due to increased rainfall. As shown in Figure 13, the actual evapotranspiration increased significantly in both seasons due to increased precipitation and soil warming. The increasing trend of the actual evapotranspiration was higher in the thawing season than in the freezing season.

Figure 14 shows the changes in the basin-averaged annual water storage in the top 0-3 m layer and the groundwater storage. The annual liquid water storage of the top 0-3 m showed a significant increasing trend especially in the most recent 3 decades. This long-term change in liquid water storage was similar to the runoff change in the freezing season, as shown in Figure 13 (a), with a correlation coefficient of 0.80. The annual ice water storage in the top 0-3 m soil showed significant decreasing trend due to frozen soils changes. Annual groundwater storage showed a significantly increasing trend

459 especially in the most recent 3 decades, which indicates that the groundwater recharge
460 increases with the frozen soil degradation.

461 **5. Discussion**

462 **5.1 Impact of frozen soil changes on the soil moisture and runoff**

463 Long-term changes of the spatially averaged liquid soil moistures in the region with
464 elevation between 3300 and 3500 m and in the region with elevation between 3500 and
465 3700 m are shown in Figure S3 in the supplement material. In the seasonally frozen
466 ground with elevation of 3300-3500 m, by comparing with the soil temperature shown
467 in Figure 12 (a), we can see that the liquid soil moisture increase was mainly caused by
468 the decrease in the frozen depth. The liquid soil moisture in the deep soil layer increased
469 significantly since the 1990s in the area with elevation of 3500-3700 m where the
470 permafrost changed to seasonally frozen ground which is shown in Figure 12 (b). This
471 indicates that the frozen soil degradation caused a significant increase in liquid soil
472 moisture in both the freezing and thawing seasons.

473 In the freezing season, since the surface ground is frozen, runoff is mainly subsurface
474 flow coming from the seasonally frozen ground. Runoff has the highest correlation
475 (r=0.82) with the liquid soil moisture in the freezing season, which indicates that the
476 frozen soils change was the major cause of the increased liquid soil moisture, resulting
477 in increased runoff in the freezing season. During the past 40 years, parts of the
478 permafrost changed into seasonally frozen ground, and the thickness of the seasonally
479 frozen ground decreased, which led to increased liquid soil moisture in the deep layers
480 during the freezing season. The increase in liquid soil moisture also increased the

hydraulic conductivity which enhanced the subsurface flow. Figure 15(c) shows the seasonal pattern of runoff in the permafrost area and seasonally frozen soils. From April to October (the thawing season), runoff in the permafrost area is much larger than in the seasonally frozen soils, but in the freezing season runoff in the permafrost area is lower than in the seasonally frozen soils. Figure S4 in the supplement material shows runoff changes from typical area (with elevation between 3500-3700 m) where covered by the permafrost in the period of 1971 to 1980 and changed into the seasonally frozen ground in the period of 2001 to 2010. This illustrates that thaw of permafrost increased the runoff in the freezing season and slowed recession processes in autumn. The increase in freezing season runoff and shift in the seasonal flow pattern are also illustrated by the model simulation without frozen soil scheme as shown in Figure S2.

In the thawing season from April to October, the thickness of the seasonally frozen ground rapidly decreased to zero and the thaw depth of permafrost reached the maximum. Runoff in the thawing season was mainly rainfall runoff, as shown in Table 2. The increased runoff mainly came from increased precipitation and snowmelt in the thawing season.

Figure 15 shows the changes in areal mean runoff along the elevation for different seasons. There was a large difference in runoff variation with the elevation between the two seasons. In the freezing season, the runoff change from the 1970s to the 2000s in the areas of seasonally frozen ground (mainly located below 3500 m, see Figure 11) was relatively small. The areas with elevations of 3500 to 3900 m showed larger changes in runoff. This is due to the shift from permafrost to seasonally frozen ground

503 in some areas in the elevation range of 3500 to 3900 m, as simulated by the model,
504 particularly for the sunny hillslopes (see Figure 11). This finding illustrates that a
505 change from the permafrost to the seasonally frozen ground has a larger impact on the
506 runoff than a change in frozen depth in the seasonally frozen ground. In the thawing
507 season, runoff increased with elevation due to the increase in precipitation with
508 increasing elevation, and the runoff increase was mainly determined by increased
509 precipitation (Gao et al., 2016). Precipitation in the region with elevation below 3100
510 m was low, but air temperature was high. Runoff in this region decreased during 2001-
511 2010 compared to 1971-1980 because of higher evapotranspiration.

512 **5.2 Comparison with the previous similar studies**

513 In this study, the model simulation showed that thaw of frozen soils led to increased
514 freezing season runoff and base flow in the upper Heihe basin. This result is consistent
515 with previous findings based on the trend analysis of streamflow observations in high
516 latitude regions (Walvoord and Striegl, 2007; Jacques and Sauchyn, 2009; Ye et al.,
517 2009) and in northeast China (Liu et al., 2003). However, those studies did not consider
518 spatial variability. This study found that the impact of the thaw of frozen soils on runoff
519 had regional characteristics. In the upper Heihe basin (see Figure 15), thaw of frozen
520 soils led to increased runoff at higher elevations but led to decreased runoff at lower
521 elevations during the freezing season. This implies that change of the freezing season
522 runoff was strongly affected by the permafrost degradation in the higher elevation
523 region but by the evaporation increase in the lower elevation region due to the air
524 temperature rising. However, runoff at the basin scale mainly came from the higher

525 elevation regions.

526 This study also showed that the thaw of frozen soils increased the soil liquid moisture
527 in the upper Heihe basin, which is consistent with the finding of Subin et al. (2013)
528 using the CLM model simulation in northern latitude permafrost regions, and the
529 findings of Cuo et al. (2015) using VIC model simulation at 13 sites on the Tibetan
530 Plateau. However, Lawrence et al. (2015) found that permafrost thawing caused soil
531 moisture drying based on CLM model simulations for the global permafrost region.
532 This might be related to the uncertainties in the soil water parameters and the high
533 spatial heterogeneity of soil properties, which are difficult to consider in a global-scale
534 model. Subin et al. (2013) and Lawrence et al. (2015) modelled the soil moisture
535 changes in the active layer of permafrost in large areas with coarse spatial resolution.
536 This study revealed the spatio-temporal variability of soil moisture with high spatial
537 resolution and analyzed the correlations with the change in frozen soils.

538 Wu and Zhang (2010) focused on the changes in the active layer thickness at 10 sites
539 in the permafrost region on the Tibetan Plateau and found a significant increasing trend
540 during the period of 1995-2007, which is consistent with the result of this study. Jin et
541 al. (2009) found decreased soil moisture and runoff due to the permafrost degradation
542 based on observations at the plot scale in the source areas in the Yellow River basin.
543 This result is different from the present study, possibly due to the difference of
544 hydrogeological structure and the soil hydraulic parameters in the source area of the
545 Yellow River from those in the upper Heihe basin. Wang et al. (2015a) focused on the
546 change in the seasonally frozen ground in the Heihe River basin based on plot

observations, and the increasing trend of the maximum frozen depth was estimated as 4.0 cm/10yr during 1972-2006, which is consistent with the GBEHM model simulation in this study. The increase in groundwater storage illustrated in this study is also consistent with the finding of Cao et al. (2012) based on the GRACE data which showed that groundwater storage increased during the period of 2003~2008 in the upper Heihe basin.

5.3 Uncertainty in simulation of the frozen soils

Estimation of the change in permafrost area is a great challenge due to such complex factors as climatology, vegetation, and geology. Guo et al. (2013) reported permafrost area for the whole Qinghai-Tibetan Plateau decreased from about 175.0×10^4 km^2 in 1981 to 151.5×10^4 km^2 with a relative change of 13.4%. Wu et al. (2005) reported that the permafrost area decreased by 12% from 1975 to 2002 in the Xidatan basin, Qinghai-Tibetan Plateau based on a ground penetration radar survey. Jin et al. (2006) found an area reduction of 35.6% in island permafrost in Liangdaohe, which is located at the southern Qinghai–Tibet Highway, from 1975 to 1996. Compared with the borehole observations by Wang et al. (2013) shown in Figure 2, this model slightly overestimated the soil temperature in permafrost areas, which might lead to overestimation of the rate of permafrost area reduction.

There were two major uncertainties in the frozen soils simulation which may lead to overestimation: uncertainty in the land surface energy balance simulation and uncertainty in the simulation of the soil heat-water transfer processes (Wu et al., 2016). Uncertainty in the land surface energy balance simulation might result from the

569 estimations of radiation and surface albedo due to the complex topography, vegetation
570 cover and soil moisture distribution, which may introduce uncertainties in the estimated
571 ground temperature and thermal heat flux into the deep layers. The uncertainty in
572 simulation of soil heat-water transfer processes might result from the soil water and
573 heat parameters and the bottom boundary condition of heat flux. For example, soil depth
574 and fraction of rock in soil may greatly affect soil temperature simulation. Permafrost
575 degradation is closely related to the thermal properties of rocks and soils, geothermal
576 flow and initial soil temperature and soil ice conditions. Figure S5 in the supplement
577 material compares the results of simulation with zero thermal flux at the lower boundary
578 and the results of simulation with thermal flux of 0.2 W/m^2 (Estimated by geothermal
579 gradient at T4 in Figure 3). It can be seen that the geothermal heat flux at the lower
580 boundary causes slight increase in soil temperature below the depth of 30 m. The lack
581 of observed initial condition data could also cause uncertainty in the permafrost change
582 estimation. Sub-grid topography effect may also affect the frozen soil simulation. For
583 example, active layer thickness is different in the low valleys and high slopes due to
584 different vegetation conditions, soil organic layers and shading by surroundings (Zhang
585 et al., 2013; O'Neill et al., 2015). This is not well considered in this study. For
586 discontinuous permafrost, lateral heat flux may increase the thawing rate (Kurylyk et
587 al., 2016; Sjöberg et al., 2016) and this effect is not considered in the present study.
588 This may lead to underestimation of thawing rates of discontinuous permafrost,
589 especially when high groundwater flow rate events occur. In addition, uncertainties
590 from input data, particularly the solar radiation which is estimated using interpolated

591 sunshine hour data from limited observational stations and precipitation which is also
592 interpolated by observations at these stations, may also influence the results of the
593 model simulation. Due to the complexity of the distributed model and large number of
594 model parameters, it is challenge to quantify overall simulation uncertainty. This work
595 will be done in the future study.

596 **6. Conclusions**

597 A distributed hydrological model coupled with cryospheric processes was carefully
598 validated in the upper Heihe River basin using available observations of soil moisture,
599 soil temperature, frozen depth, actual evaporation and streamflow discharge. Based on
600 the model simulations from 1971 to 2013 in the upper Heihe River, the long-term
601 changes in frozen soils were investigated, and the effect of the frozen soils change on
602 hydrological processes were explored. Based on these analyses, the following
603 conclusions can be drawn:

604 (1) The model simulation suggests that 9.5% of permafrost areas degraded into
605 seasonally frozen grounds in the upper Heihe River basin during the period of 1971 to
606 2013, which predominantly occurred at the elevations between 3500 m and 3900 m.
607 The decreasing trend of annual maximum frozen depth is estimated to be 5.2 cm/10yr
608 for the seasonally frozen grounds, which is consistent with previous observation-based
609 studies at plot scale. The increasing trend of active layer thickness is estimated to be
610 3.5 cm/10yr in the permafrost regions.

611 (2) Model simulated trends in runoff agree with the observed trends. In the freezing
612 season (November-March), based on the model simulation, runoff was mainly sourced

by subsurface flow which increased significantly in the higher elevation regions where significant frozen soil changes occurred. This finding implies that runoff increase in the freezing season is primarily caused by frozen soil changes (permafrost degradation and decrease of the seasonally frozen depth). In the thawing season (April-October), model simulation indicates that runoff mainly came from rainfall and showed an increasing trend at the higher elevations, which can be explained by the increased precipitation. In both the freezing and thawing seasons, model simulated runoff decreased in the lower elevation region, which can be explained by increased evaporation due to the rising air temperature.

(3) Model simulated changes in soil moisture and soil temperature indicates that annual storage of the liquid water increased especially in the most recent three decades, due to the change in frozen soils. Annual ice water storage in the top 0-3 m of soil showed a significant decreasing trend due to soil warming. Model simulated annual groundwater storage had an increasing trend, which is consistent with the changes observed by the GRACE satellite. This indicated that groundwater recharge in the upper Heihe basin was enhanced in recent decades.

(4) Model simulation indicated that regions where the permafrost changed into the seasonally frozen ground had larger changes in runoff and soil moisture than the areas covered by seasonally frozen ground.

For a better understanding of changes in frozen soils and their impact on ecohydrology, the interactions among the soil freezing-thawing processes, vegetation dynamics and hydrological processes need to be investigated in future studies. There

635 are uncertainties in simulations of the frozen soils and the hydrological processes that
636 might be related to the soil properties, the high spatial heterogeneity, and the assumption
637 of zero geothermal heat flux at the lower boundary, all of which warrant further
638 investigation in the future.
639
640 **Acknowledgements:** This research was supported by the major plan of "Integrated
641 Research on the Ecohydrological Processes of the Heihe Basin" (Project Nos.
642 91225302 and 91425303) funded by the National Natural Science Foundation of China
643 (NSFC). The authors would like to thank the editor and two anonymous reviewers for
644 their constructive comments, which greatly improved the manuscript.
645
646 **References**
647 Bartelt P. and M. Lehning: A physical snowpack model for the swiss avalanche warning: Part Ⅰ:
648 numerical model, Cold Regions Sci. and Tech., 35(3), 123-145, doi: 10.1016/S0165-
649 232X(02)00074-5, 2002.
650 Cao Y., Nan Z. and Hu X.: Estimating groundwater storage changes in the Heihe river basin using
651 GRACE, in: IEEE International Geoscience and Remote Sensing Symposium (IGARSS), Munich,
652 Germany, 22–27 July 2012, 798-801, 2012.
653 Chen, R., Lu, S., Kang, E., Ji, X., Zhang, Z., Yang, Y., Qing, W.: A distributed water-heat coupled model
654 for mountainous watershed of an inland river basin of Northwest China (I) model structure and
655 equations, Environ. Geol., 53, 1299-1309, doi: 10.1007/s00254-007-0738-2,2008.
656 Cheng, G. and Jin, H.: Permafrost and groundwater on the Qinghai-Tibet Plateau and in northeast China,

Hydrogeol. J., 21, 5-23, doi: 10.1007/s10040-012-0927-2, 2013.

Cheng, G., Li, X., Zhao, W., Xu, Z., Feng, Q., Xiao, S., Xiao, H.: Integrated study of the water-ecosystem-economy in the Heihe River Basin. Nat. Sci. Rev., 1(3), 413-428, doi: 10.1093/nsr/nwu017, 2014.

Cheng, G., and Wu T.: Responses of permafrost to climate change and their environmental significance, Qinghai-Tibet Plateau, J. Geophys. Res., 112, F02S03, doi:10.1029/2006JF000631, 2007.

Cherkauer, K. A., and D. P. Lettenmaier: Hydrologic effects of frozen soils in the upper Mississippi River basin, J. Geophys. Res., 104, 19,599-19,610, doi: 10.1029/1999JD900337, 1999.

Cong Z T, Yang D W, Gao B, et al.: Hydrological trend analysis in the Yellow River basin using a distributed hydrological model, Water Resour Res, 45: W00A13, doi: 10.1029/2008WR006852, 2009

Cuo, L., Y. Zhang, F. Zhu, and L. Liang.: Characteristics and changes of streamflow on the Tibetan Plateau: A review, J. Hydrol.: Reg. Stud., 2, 49-68, doi: 10.1016/j.ejrh.2014.08.004, 2014.

Cuo, L., Y. Zhang, T. J. Bohn, L. Zhao, J. Li, Q. Liu, and B. Zhou: Frozen soil degradation and its effects on surface hydrology in the northern Tibetan Plateau, J. Geophys. Res. Atmos., 120, doi:10.1002/2015JD023193, 2015.

Duan L., Man X., Kurylyk B. L. and Cai T.: Increasing winter baseflow in response to permafrost thaw and precipitation regime shifts in northeastern China, Water, 9(1), 25, doi:10.3390/w9010025, 2017.

Endrizzi S, Gruber S, Dall'Amico M, and R. Rigon: GEOtop 2.0: simulating the combined energy and water balance at and below the land surface accounting for soil freezing, snow cover and terrain effects, Geosci. Model Dev., 7: 2831-2857, doi:10.5194/gmd-7-2831-2014, 2014.

Fan, W.: Heihe 1km LAI production, Heihe Plan Science Data Center at Lanzhou,

679 doi:10.3972/heihe.090.2014.db, 2014.
680 Farouki, O.T.: The thermal properties of soils in cold regions, Cold Regions Sci.and Tech., 5, 67-75, doi:
681 10.1016/0165-232X(81)90041-0, 1981.
682 Flerchinger G., Saxton K.: Simultaneous heat and water model of a freezing snow-residue-soil system I.
683 Theory and development, Trans. ASAE, 32, 565-571, doi: 10.13031/2013.31040, 1989.
684 Gao B., Qin Y., Wang YH, Yang DW, and Zheng YR: Modeling Ecohydrological Processes and Spatial
685 Patterns in the Upper Heihe Basin in China, Forests, 7(1),10, doi:10.3390/f7010010, 2016.
686 Guo, D., and H. Wang: Simulation of permafrost and seasonally frozen ground conditions on the Tibetan
687 Plateau, 1981–2010, J. Geophys. Res. Atmos., 118, 5216-5230, doi:10.1002/jgrd.50457, 2013.
688 Hinzman, L.D., C.J. Deal, A.D. McGuire, S.H. Mernild, I.V. Polyakov, and J.E. Walsh: Trajectory of
689 the Arctic as an integrated system, Ecol. Appl., 23(8),1837-1868, doi:10.1890/11-1498.1, 2013.
690 Jacques St., J.-M., and Sauchyn D. J.: Increasing winter baseflow and mean annual streamflow from
691 possible permafrost thawing in the Northwest Territories, Canada, Geophys. Res. Lett., 36, L01401,
692 doi:10.1029/2008GL035822, 2009.
693 Jarvis, A., Reuter, H.I., Nelson, A., Guevara, E.: Hole-filled seamless SRTM data, Version 4,
694 International Centre for Tropical Agriculture (CIAT), 2008.
695 Jin, H., He, R., Cheng, G., Wu, Q., Wang, S., Lu, L. and Chang X.: Changes in frozen ground in the
696 Source Area of the Yellow River on the Qinghai–Tibet Plateau, China, and their eco-environmental
697 impacts, Environ. Res. Lett., 4(4), 045206, doi:10.1088/1748-9326/4/4/045206, 2009.
698 Jin, H.J., Zhao, L., Wang, S.L., Jin, R.: Thermal regimes and degradation modes of permafrost along
699 the Qinghai–Tibet Highway, Science in China D: Earth Sciences, 49 (11), 1170-1183, 2006.
700 Jordan R.: A one-dimensional temperature model for a snow cover, Technical Documentation for

SNTHERM.89, Cold Regions Research and Engineering Lab, Hanover NH, 49 pp., 1991.

Kurylyk, B. L., M. Hayashi, W. L. Quinton, J. M. McKenzie, and C. I. Voss: Influence of vertical and lateral heat transfer on permafrost thaw, peatland landscape transition, and groundwater flow, Water Resour. Res., 52, 1286-1305, doi:10.1002/2015WR018057, 2016.

Lawrence, D.M., C.D. Koven, S.C. Swenson, W.J. Riley, and A.G. Slater: Permafrost thaw and resulting soil moisture changes regulate projected high-latitude CO_2 and CH_4 emissions, Environ. Res. Lett., 10, doi:10.1088/1748-9326/10/9/094011, 2015.

Li, D.L., Zhong, H.L., Wu, Q.B., Zhang, Y.J., Hou, Y.L., Tang, M.C.: Analyses on changes of surface temperature over Qinghai–Xizang Plateau, Plateau Meteorology, 24, 291-298, 2005 (in Chinese).

Li, X., Cheng, G.D., Liu, S.M., Xiao, Q., Ma, M.G., Jin, R., Che, T., Liu, Q.H., Wang, W.Z., Qi, Y., Wen, J.G., Li, H.Y., Zhu, G.F., Guo, J.W., Ran, Y.H., Wang, S.G., Zhu, Z.L., Zhou, J., Hu, X.L., Xu, Z.W.: Heihe Watershed Allied Telemetry Experimental Research (HiWATER): Scientific Objectives and Experimental Design, B. Am. Meteorol. Soc., 94(8), 1145-1160, doi: 10.1175/BAMS-D-12-00154.1, 2013.

Liu, X. and Chen, B.: Climate warming in the Tibetan Plateau during recent decades, Int. J. Climatol., 20(1), 1729-1742, doi: 10.1002/1097-0088(20001130)20:14<1729::AID-JOC556>3.0.CO;2-, 2000.

Liu, S., Xu Z., Wang W., Bai J., Jia Z., Zhu M., and Wang J.: A comparison of eddy-covariance and large aperture scintillometer measurements with respect to the energy balance closure problem, Hydrol. Earth Syst. Sc., 15(4), 1291-1306, doi:10.5194/hess-15-1291-2011, 2011.

Liu J., N. Hayakawab, Lu M., Dong S., and Yuan J.: Hydrological and geocryological response of winter streamflow to climate warming in Northeast China, Cold Regions Sci.and Tech., 37,15-24, doi: 10.1016/S0165-232X(03)00012-0, 2003.

Wu T., Li S., Cheng G. and N Z.: Using ground-penetrating radar to detect permafrost degradation in the northern limit of permafrost on the Tibetan Plateau, Cold Regions Sci.and Tech., 41, 211-219, 2005, doi:10.1016/j.coldregions.2004.10.006.

Niu L., Ye B., Li J., and Sheng Y.: Effect of permafrost degradation on hydrological processes in typical basins with various permafrost coverage in Western China, China Earth Sci., 54(4), 615-624, doi: 10.1007/s11430-010-4073-1, 2011.

Oerlemans, J. and Knap, W.H.: A 1 year record of global radiation and albedo in the ablation zone of Morteratschgletscher, Switzerland, J. Glaciol., 44, 231-238, doi: 10.3198/1998JoG44-147-231-238, 1998.

Oerlemans, J.: Glaciers and Climate Change, Lisse: Swets & Zeitlinger, 2001.

Oleson, K.W., Lawrence, D.M., Bonan, G.B., Flanner, M.G., Kluzek, E., Lawrence, P.J., Levis, S., Swenson, S.C., Thornton, P.E., Dai, A., Decker, M., Dickinson, R., Feddema, J., Heald, C.L., Hoffman, F., Lamarque, J., Mahowald, N., Niu, G., Qian, T., Randerson, J., Running, S., Sakaguchi, K., Slater, A., Stöckli, R., Wang, A., Yang, Z., Zeng, X., Zeng, X.: Technical Description of version 4.0 of the Community Land Model (CLM), NCAR Technical Note NCAR/TN-47+STR, National Center for Atmospheric Research, Boulder, CO, 257 pp., 2010.

Qiu J.: Thawing permafrost reduces river runoff, Nature, doi:10.1038/nature.2012.9749, 2012.

Ou, C., B. Leblon, Y. Zhang, A. LaRocque, K. Webster, and J. McLaughlin: Modelling and mapping permafrost at high spatial resolution using Landsat and RADARSAT images in northern Ontario, Canada: Part 1 - Model calibration, International Journal of Remote Sensing, doi: 10.1080/01431161.2016.1157642, 2016.

O'Neill, H. B., Burn, C. R., Kokelj, S. V. & Lantz, T. C.: 'Warm' tundra: atmospheric and near-surface ground temperature inversions across an alpine treeline in continuous permafrost, western arctic, Canada. Permafrost and Periglac. Process. 26, 103–118, doi: 10.1002/ppp.1838., 2015.

Rawlins M., Lammers R., Frolking S., Fekete B. and Vorosmarty C.: Simulating pan-Arctic runoff with

748 a macro-scale terrestrial water balance model, Hydrol. Process., 17, 2521-2539, doi:
749 10.1002/hyp.1271, 2003.
750 Rawlins, M.A., D.J. Nicolsky, K.C. McDonald, and V.E. Romanovsky: Simulating soil freeze/thaw
751 dynamics with an improved pan-Arctic water balance model, J. Adv. Model. Earth Syst., 5:659-675,
752 doi:10.1002/jame.20045, 2013.
753 Rigon R., Bertoldi G., and Over TM: GEOtop: A distributed hydrological model with coupled water
754 and energy budgets, J. Hydrometeorol., 7, 371–388, doi: 10.1175/JHM497.1, 2006.
755 Schuur, E.A.G., A.D. McGuire, C. Schädel, G. Grosse, J.W. Harden, D.J. Hayes, G. Hugelinus, C.D.
756 Koven, P. Kuhry, D.M. Lawrence, S.M. Natali, D. Olefeldt, V.E. Romanovsky, K. Schaefer, M.R.
757 Turetsky, C.C. Treat, and J.E. Vonk: Climate change and the permafrost carbon feedback, Nature
758 520,171-179 doi:10.1038/nature14338, 2015.
759 Sellers, P.J.: Canopy reflectance, photosynthesis, and transpiration, Int. J. Remote Sens., 8, 1335-1372,
760 doi: 10.1080/01431168508948283, 1985.
761 Sellers, P.J.; Randall, D.A.; Collatz, G.J.; Berry, J.A.; Field, C.B.; Dazlich, D.A.; Zhang, C.; Collelo,
762 G.D.; Bounoua, L.: A Revised Land Surface Parameterization (SiB2) for Atmospheric GCMS.
763 Part I: Model Formulation, J. Clim., 9, 676-705, doi: 10.1175/1520-
764 0442(1996)009<0676:ARLSPF>2.0.CO;2, 1996.
765 Sjöberg, Y., E. Coon, A. B. K. Sannel, R. Pannetier, D. Harp, A. Frampton, S. L. Painter, and S. W. Lyon:
766 Thermal effects of groundwater flow through subarctic fens: A case study based on field
767 observations and numerical modeling, Water Resour. Res., 52, 1591-1606,
768 doi:10.1002/2015WR017571, 2016.
769 Song X., Brus DJ, Liu F., Li D., Zhao Y., Yang J. and Zhang G.: Mapping soil organic carbon content by

geographically weighted regression: A case study in the Heihe River Basin, China, Geoderma, 261,11–22, doi: 10.1016/j.geoderma.2015.06.024, 2016.

Strahler A N: Quantitative analysis of watershed geomorphology, Eos, Transactions American Geophysical Union, 38(6), 913-920, doi: 10.1029/TR038i006p00913, 1957.

Subin Z.M., Koven C.D., Riley W.J., Torn M.S., Lawrence D.M. and Swenson S.C.: Effects of Soil Moisture on the Responses of Soil Temperatures to Climate Change in Cold Regions, J. Clim., 26,3139-3158, doi: 10.1175/JCLI-D-12-00305.1, 2013.

Toon, O.B., McKay, C.P., Ackerman, T.P., and Santhanam, K.: Rapid calculation of radiative heating rates and photodissociation rates in inhomogeneous multiple scattering atmospheres, J. Geophys. Res. 94(D13), 16,287-16,301, doi: 10.1029/JD094iD13p16287, 1989.

Walter W. Immerzeel, Ludovicus P. H. van Beek, and Marc F. P. Bierkens.: Climate Change Will Affect the Asian Water Towers, Science, 328, 1382-1385, doi: 10.1126/science.1183188, 2010.

Walvoord, M. A. and B. L. Kurylyk: Hydrologic Impacts of Thawing Permafrost—A Review, Vadose Zone J., doi:10.2136/vzj2016.01.0010, 2016.

Walvoord, M. A., and R. G. Striegl: Increased groundwater to stream discharge from permafrost thawing in the Yukon River basin: Potential impacts on lateral export of carbon and nitrogen, Geophys. Res. Lett., 34, L12402, doi:10.1029/2007GL030216, 2007.

Wang, L., Koike, T., Yang, K., Jin, R., Li, H.: Frozen soil parameterization in a distributed biosphere hydrological model, Hydrol. Earth Syst. Sc., 14(3), 557-571, doi: 10.5194/hess-14-557-2010, 2010.

Wang Q., Zhang T., Wu J., et al.: Investigation of permafrost distribution over the upper reaches of the Heihe River in the Qilian Mountains, Journal of Glaciology and Geocryology, 35(1), 19-29, 2013 (in Chineses).

792 Wang Q., Zhang T., Peng X., Cao B., and Wu Q.: Changes of soil thermal regimes in the Heihe River
793 Basin over Western China, Arct., Antarct., and Alpine Res., 47(2), 231-241, doi:
794 10.1657/AAAR00C-14-012, 2015a.
795 Wang, Y., Yang, D., Lei, H. and Yang, H.: Impact of cryosphere hydrological processes on the river runoff
796 in the upper reaches of Heihe River, J. Hydraul. Eng., 46, 1064-1071, 2015b (In Chinese).
797 Wang, Y., Yang, H., Yang, D., Qin Y., Gao B. and Cong ZT.: Spatial interpolation of daily precipitation
798 in a high mountainous watershed based on gauge observations and a regional climate model
799 simulation, J. Hydrometeorol.,18, 845-862, 2017, doi: 10.1175/JHM-D-16-0089.1.
800 Woo, M.-K., Kane, D. L., Carey, S. K. and Yang, D.: Progress in permafrost hydrology in the new
801 millennium, Permafrost Periglac. Process., 19, 237-254, doi:10.1002/ppp.613, 2008.
802 Woo M K.: Permafrost Hydrology, Springer-Verlag, Berlin Heidelberg, 2012.
803 Wu, B.F., Yan, N.N., Xiong, J., Bastiaanssen, W., Zhu, W.W., Stein, A.: Validation of ETWatch using
804 field measurements at diverse landscapes: A case study in Hai Basin of China. J. Hydrol., 436, 67-
805 80, doi: 10.1016/j.jhydrol.2012.02.043, 2012.
806 Wu, B.F.: Monthly Evapotranspiration Datasets (2000–2012) with 1 km Spatial Resolution over the
807 Heihe River Basin, Heihe Plan Science Data Center at Lanzhou, China, doi:
808 10.3972/heihe.115.2013.db, 2013.
809 Wu, M., Jansson P. E., Tan X., Wu J., and Huang, J.: Constraining parameter uncertainty in simulations
810 of water and heat dynamics in seasonally frozen soil using limited observed data, Water, 8(2), 64,
811 doi:10.3390/w8020064, 2016.
812 Wu, Q., and Zhang T.: Changes in active layer thickness over the Qinghai-Tibetan Plateau from 1995 to
813 2007, J. Geophys. Res., 115, D09107, doi: 10.1029/2009JD012974, 2010.

814 Yang, D.W., Gao, B., Jiao, Y., Lei, H.M., Zhang, Y.L., Yang, H.B., Cong, Z.T.: A distributed scheme
815 developed for eco-hydrological modeling in the upper Heihe River, China Earth Sci., 58(1), 36-45,
816 doi: 10.1007/s11430-014-5029-7, 2015.
817 Yang, D.W., Herath, S., and Musiake, K.: Development of a geomorphology-based hydrological model
818 for large catchments, Annu. J. Hydraul. Eng., 42, 169-174, doi: 10.2208/prohe.42.169, 1998.
819 Yang, D.W., Herath, S., and Musiake, K.: A hillslope-based hydrological model using catchment area
820 and width functions, Hydrol. Sci. J., 47, 49-65, doi: 10.1080/02626660209492907, 2002.
821 Yang, M., F. E. Nelson, N. I. Shiklomanov, D. Guo, and G. Wan, Permafrost degradation and its
822 environmental effects on the Tibetan Plateau: A review of recent research, Earth Sci. Rev., 103, 31-
823 44, doi: 10.1016/j.earscirev.2010.07.002, 2010.
824 Ye, B., D. Yang, Z. Zhang, and D. L. Kane: Variation of hydrological regime with permafrost coverage
825 over Lena Basin in Siberia, J. Geophys. Res., 114, D07102, doi:10.1029/2008JD010537, 2009.
826 Zhao, L., C. L. Ping, D. Q. Yang, G. D. Cheng, Y. J. Ding, and S. Y. Liu: Changes of climate and
827 seasonally frozen ground over the past 30 years in Qinghai-Xizang (Tibetan) Plateau, China, Global
828 Planet. Change, 43, 19-31, doi: 10.1016/j.gloplacha.2004.02.003, 2004.
829 Zhang, Y.L., Cheng, G.D., Li, X., Han, X.J., Wang, L., Li, H.Y., Chang, X.L., Flerchinger, G.N.:
830 Coupling of a simultaneous heat and water model with a distributed hydrological model and
831 evaluation of the combined model in a cold region watershed, Hydrol. Process., 27(25), 3762-3776,
832 doi: 10.1002/hyp.9514, 2013.
833 Zhang, Y., Ohata, T., and Kadota, T.: Land-surface hydrological processes in the permafrost region of the
834 eastern Tibetan Plateau, J. Hydrol., 283, 41-56, doi: 10.1016/S0022-1694(03)00240-3, 2003.
835 Zhang, Y., X. Wang, R. Fraser, I. Olthof, W. Chen, D. Mclennan, S. Ponomarenko, and W. Wu: Modelling

and mapping climate change impacts on permafrost at high spatial resolution for an Arctic region with complex terrain, The Cryosphere, 7, 1121-1137, doi:10.5194/tc-7-1121-2013, 2013. Zhou, J.H. and Zheng, Y.R.: Vegetation Map of the upper Heihe basin, Version 2.0, Heihe Plan Science Data Center at Lanzhou, China, doi:10.3972/heihe.426.2014.db, 2014.

842 **Figure caption:**

843 Figure 1. The Study area, hydrological stations, borehole observation and flux tower stations

844 Figure 2. Model structure and vertical discretization of soil column

845 Figure 3. Comparison of the simulated and the observed soil temperature at borehole observation
846 sites, and the observed data is provided by Wang et al. (2013)

847 Figure 4. Daily soil temperature at the Qilian station: (a) observation; (b) simulation; (c) Simulation-
848 Observation

849 Figure 5. Comparison of the simulated and observed daily frozen depths during the period of 2002-
850 2014 at: (a) the Qilian station, (b) the Yeniugou station

851 Figure 6. Comparison of the simulated and the observed hourly liquid soil moisture at the A'rou
852 Sunny Slope station

853 Figure 7. Figure 7. Comparison of the simulated and the observed daily river discharge at: (a) the
854 Yingluoxia Gauge, (b) the Qilian Gauge, and (c) the Zhamashike Gauge (The upper panel is
855 calibration period, and the bottom panel is the validation period for each gauge))

856 Figure 8. Comparison of the simulated and the remote sensing estimated actual evapotranspiration
857 provided by Wu (2013) in the period of 2002~2012

858 Figure 9. Changes of the mean soil temperature in different seasons: (a) the freezing season (from
859 November to March) (b) the thawing season (from April to October)

860 Figure 10. Change of the frozen soils in the upper Heihe basin: (a) areas of permafrost and basin
861 averaged annual air temperature; (b) the basin averaged annual maximum frozen depth of the
862 seasonally frozen ground and the annual maximum thaw depth of the permafrost

863 Figure 11. Distribution of permafrost and seasonally frozen ground: (a) distribution in the period of

1971-1980; (b) distribution in the period of 2001-2010; (c) Areas where where permafrost changed into seasonally frozen ground (d) percentage of areas of permafrost on sunny slope; (e) percentage of areas of permafrost on shaded slope (the same legend as (d))

Figure 12. Spatial averaged monthly soil temperature during the period of 1971-2013 in different elevation intervals: (a) the seasonally frozen ground with elevation between 3300-3500 m; (b) the areas where permafrost changed to seasonally frozen ground with elevation between 3500-3700 m

Figure 13. Changes of the runoff and actual evapotranspiration: (a) in the freezing season; (b) in the thawing season

Figure 14. Changes of the annual water storage (equivalent water depth) during the period of 1971-2013: (a) the liquid soil water storage of the top 0-3 m layer; (b) the ice water storage of the top 0-3 m layer; (c) the groundwater storage

Figure 15. Model simulated runoff change with elevation: (a) in the freezing season, (b) in the thawing season, and (c) seasonal pattern of the runoff in the permafrost areas and in the seasonally frozen ground areas in the period of 2001-2010.

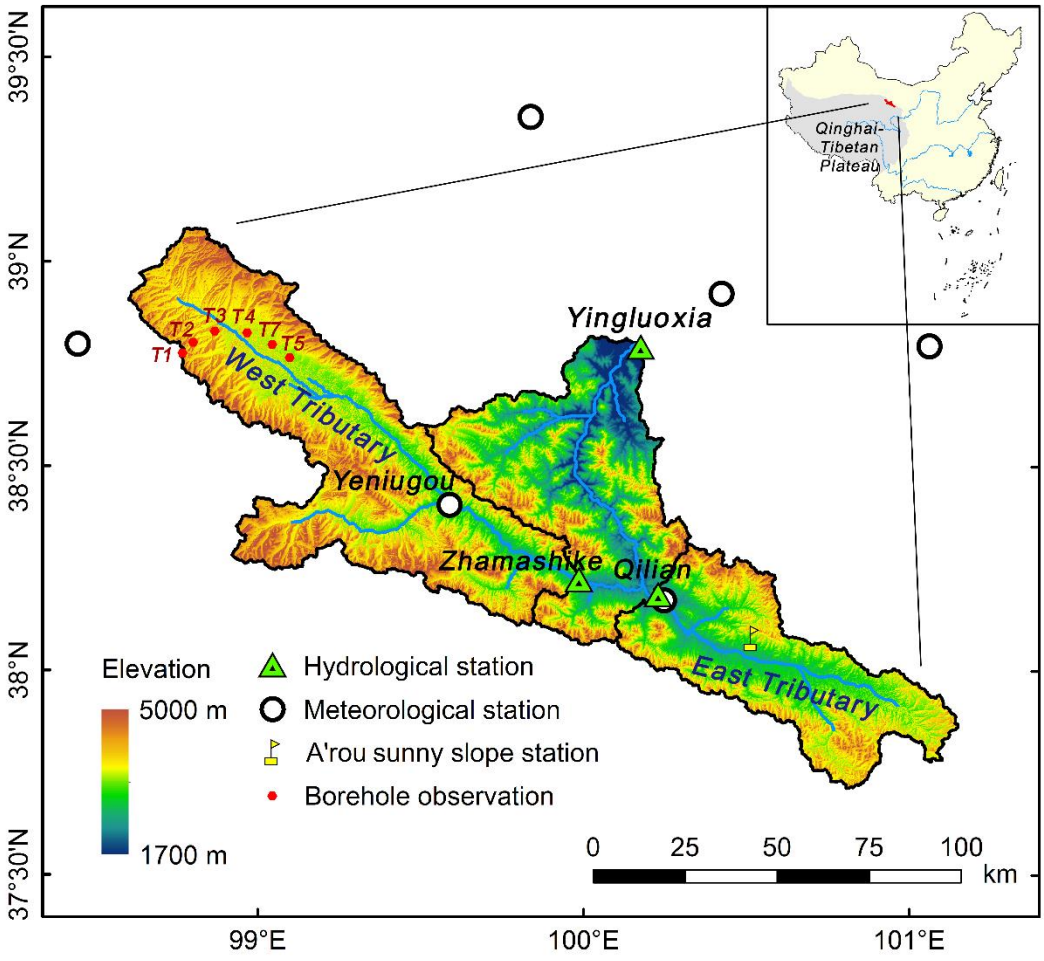

Figure 1. The Study area, hydrological stations, borehole observation and flux tower stations

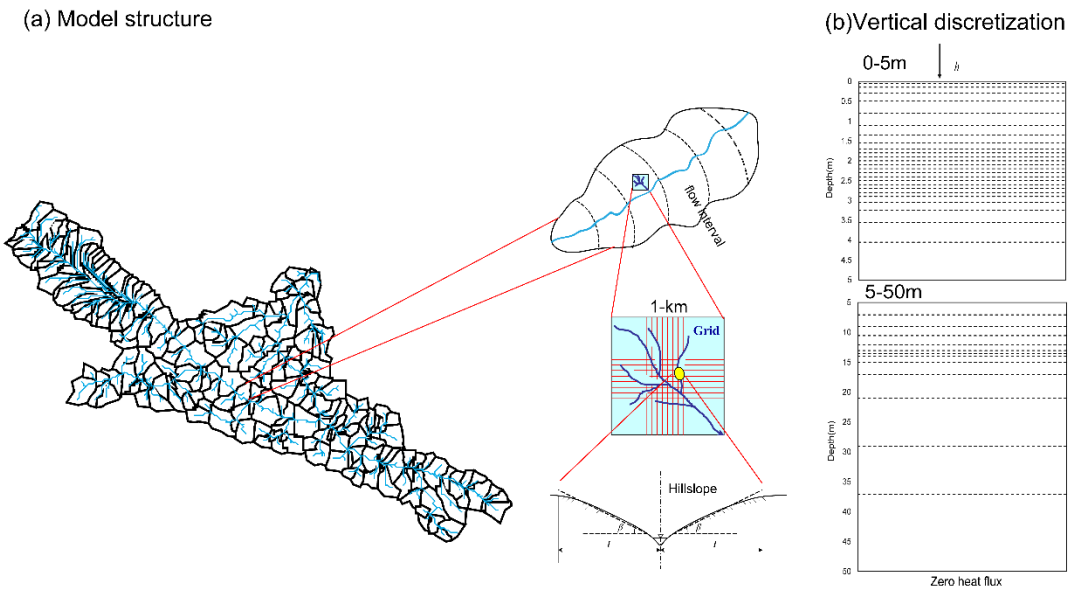

884

885 Figure 2. Model structure and vertical discretization of soil column

886

887

888

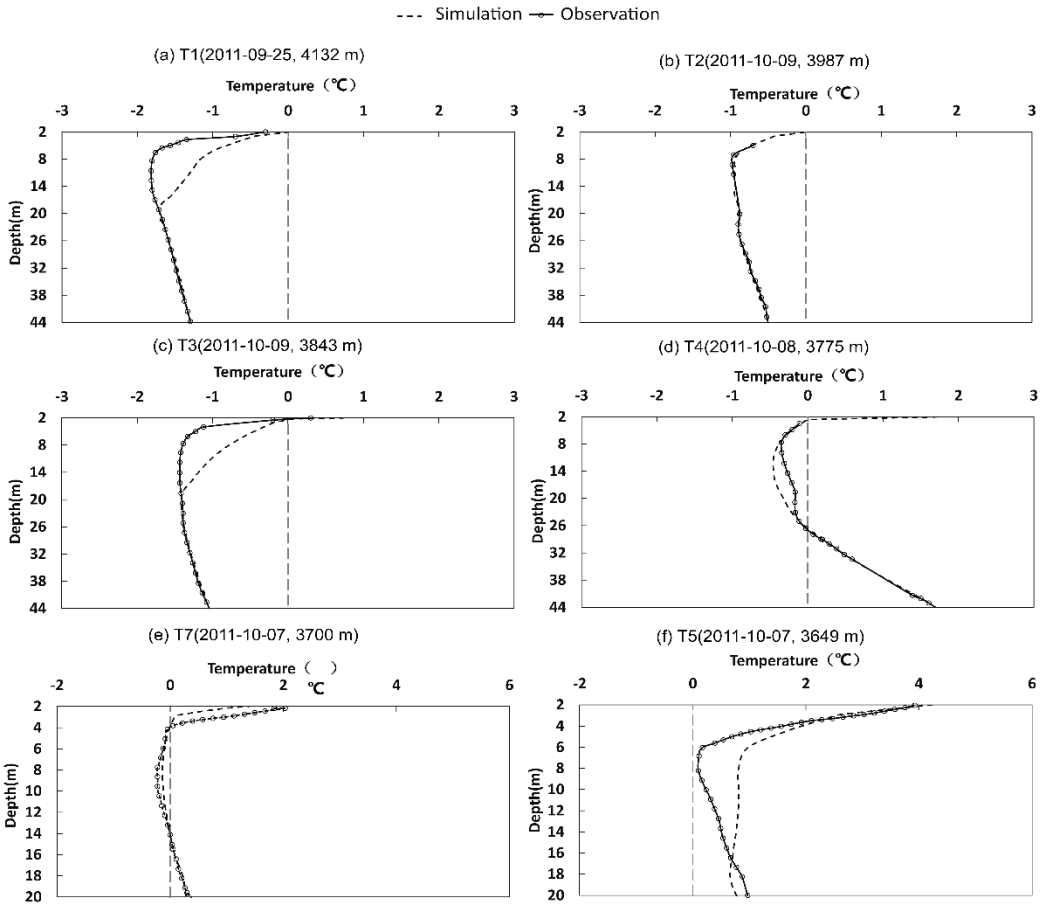

Figure 3. Comparison of the simulated and the observed soil temperature at borehole observation sites, and the observed data is provided by Wang et al. (2013)

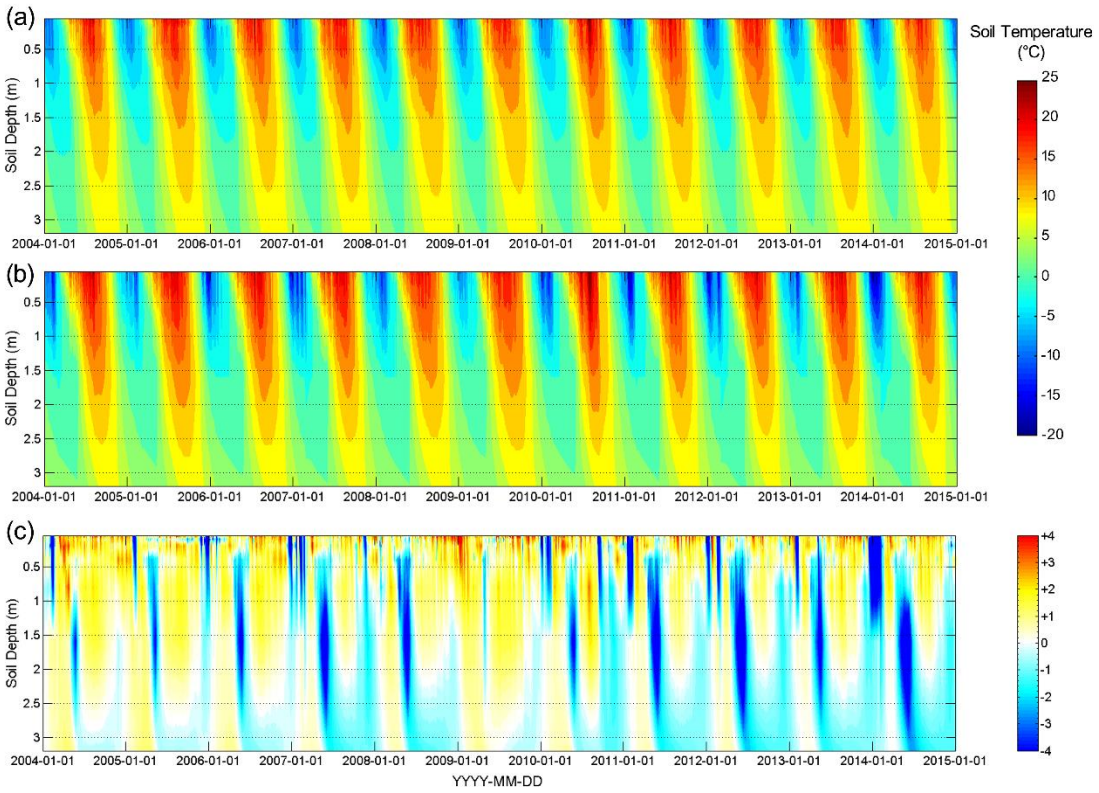

892

893 Figure 4 Daily soil temperature at the Qilian station: (a) observation; (b) simulation;

894 (c) Simulation-Observation

895

896

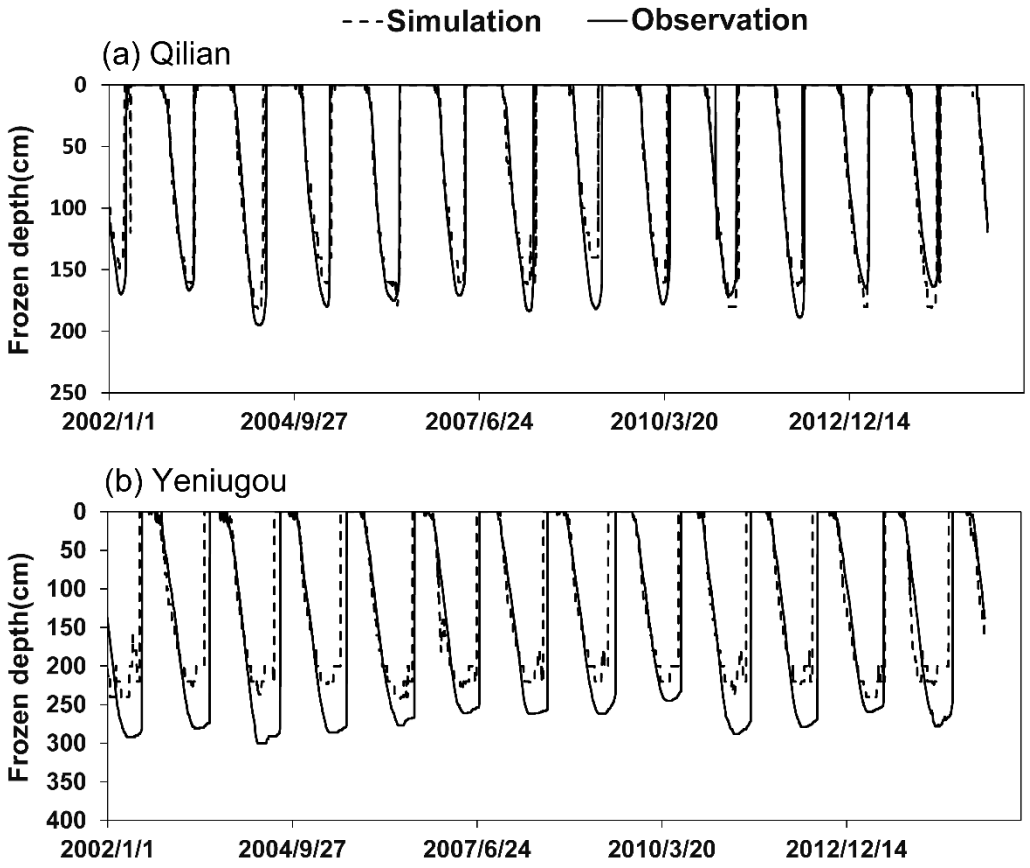

897

898 Figure 5. Comparison of the simulated and observed daily frozen depths during the

899 period of 2002-2014 at: (a) the Qilian station, (b) the Yeniugou station

900

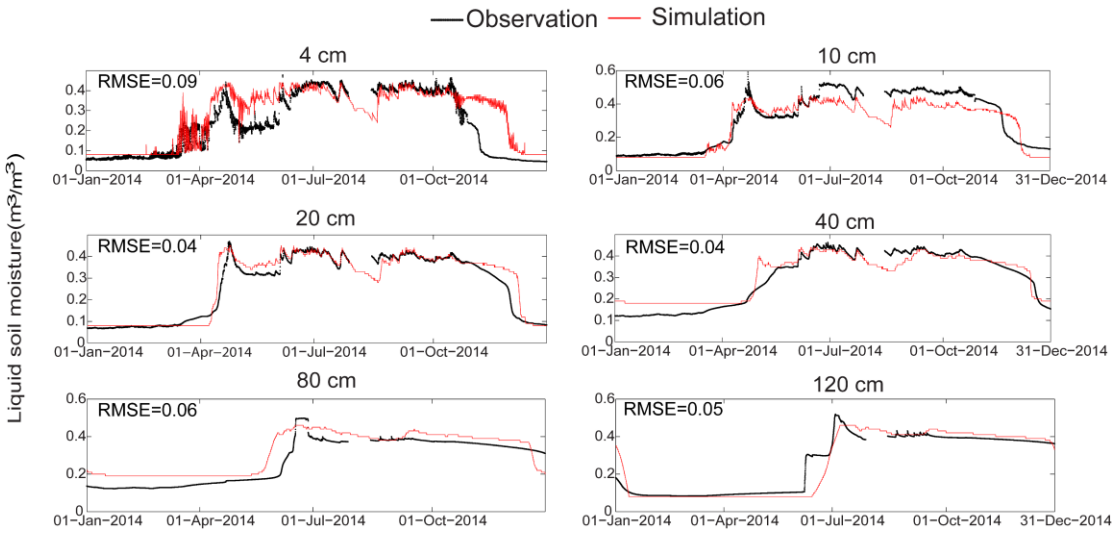

901

902 Figure 6. Comparison of the simulated and the observed hourly liquid soil moisture at

903 the A'rou Sunny Slope station

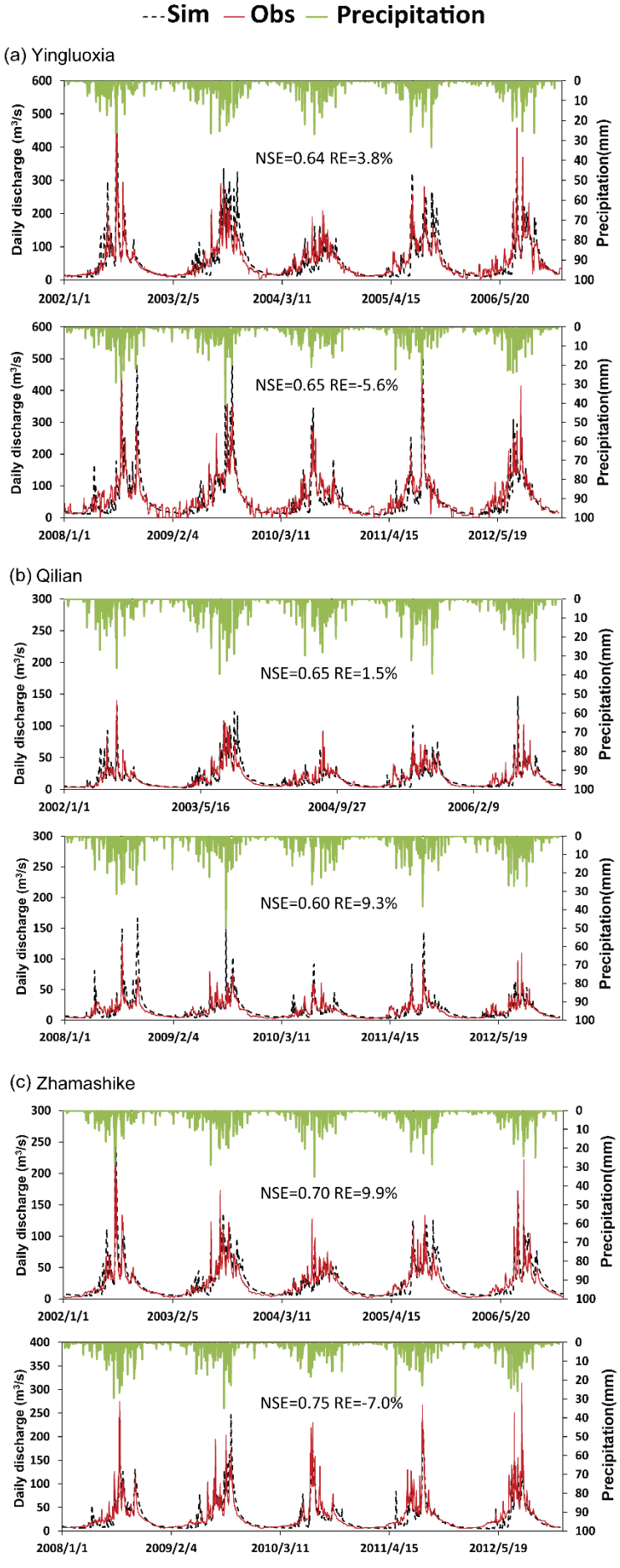
---Sim — Obs — Precipitation
(a) Yingluoxia
NSE=0.64 RE=3.8%
NSE=0.65 RE=-5.6%
(b) Qilian
NSE=0.65 RE=1.5%
NSE=0.60 RE=9.3%
(c) Zhamashike
NSE=0.70 RE=9.9%
NSE=0.75 RE=-7.0%
Daily discharge (m³/s)
Precipitation(mm)
2002/1/1
2003/2/5
2004/3/11
2005/4/15
2006/5/20
2008/1/1
2009/2/4
2010/3/11
2011/4/15
2012/5/19
2002/1/1
2003/5/16
2004/9/27
2006/2/9

904

Figure 7. Comparison of the simulated and the observed daily river discharge at: (a) the Yingluoxia Gauge, (b) the Qilian Gauge, and (c) the Zhamashike Gauge (The upper panel is calibration period, and the bottom panel is the validation period for each gauge)).

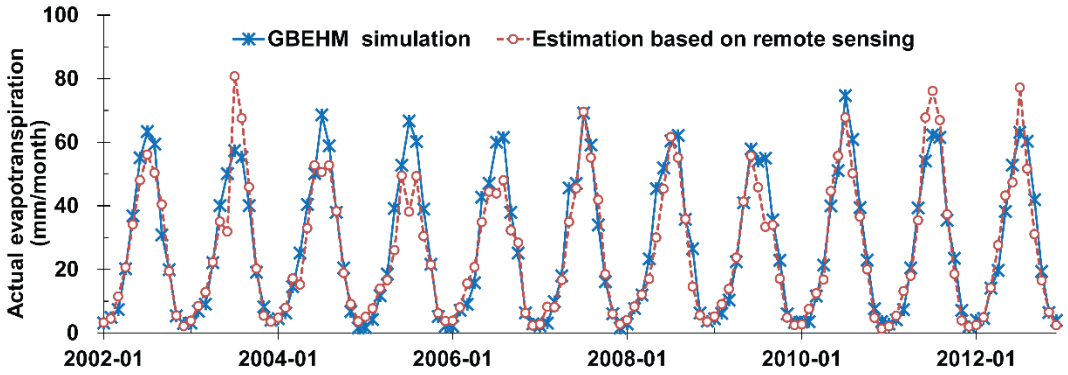

Figure 8. Comparison of the simulated and the remote sensing estimated actual evapotranspiration provided by Wu (2013) in the period of 2002~2012

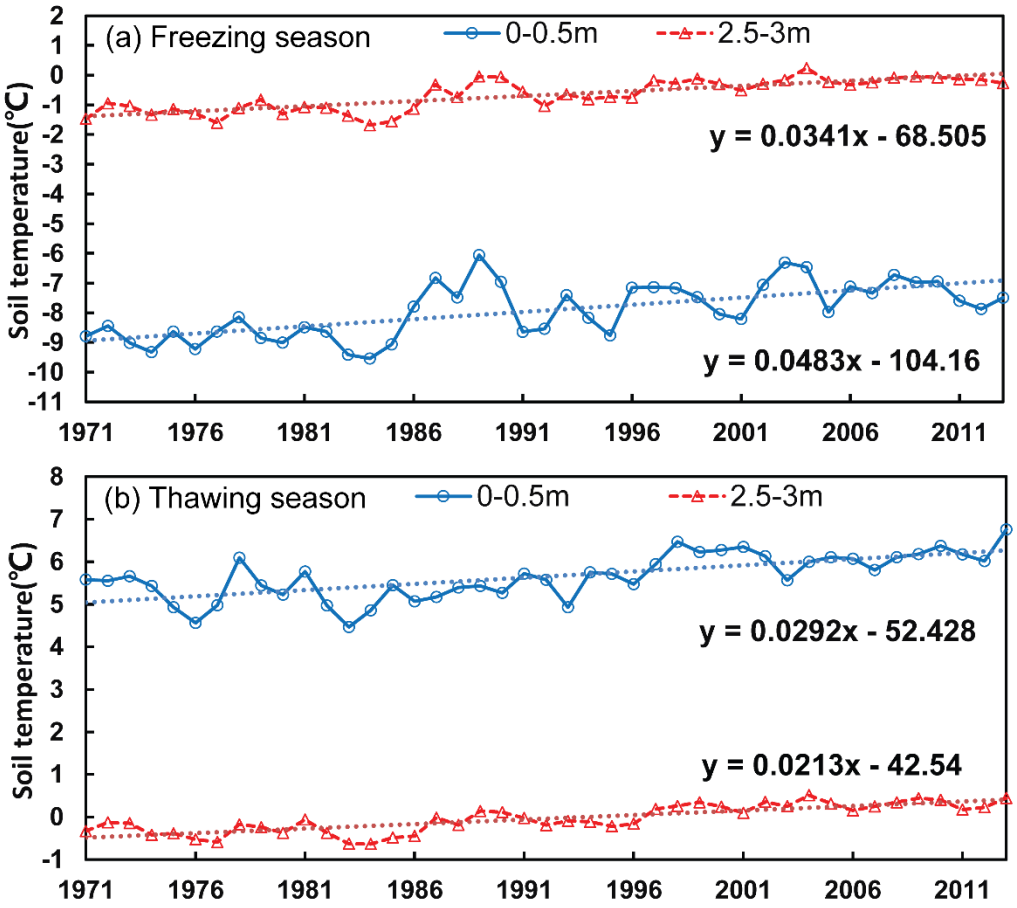

Figure 9. Changes of the mean soil temperature in different seasons: (a) the freezing season (from November to March) (b) the thawing season (from April to October)

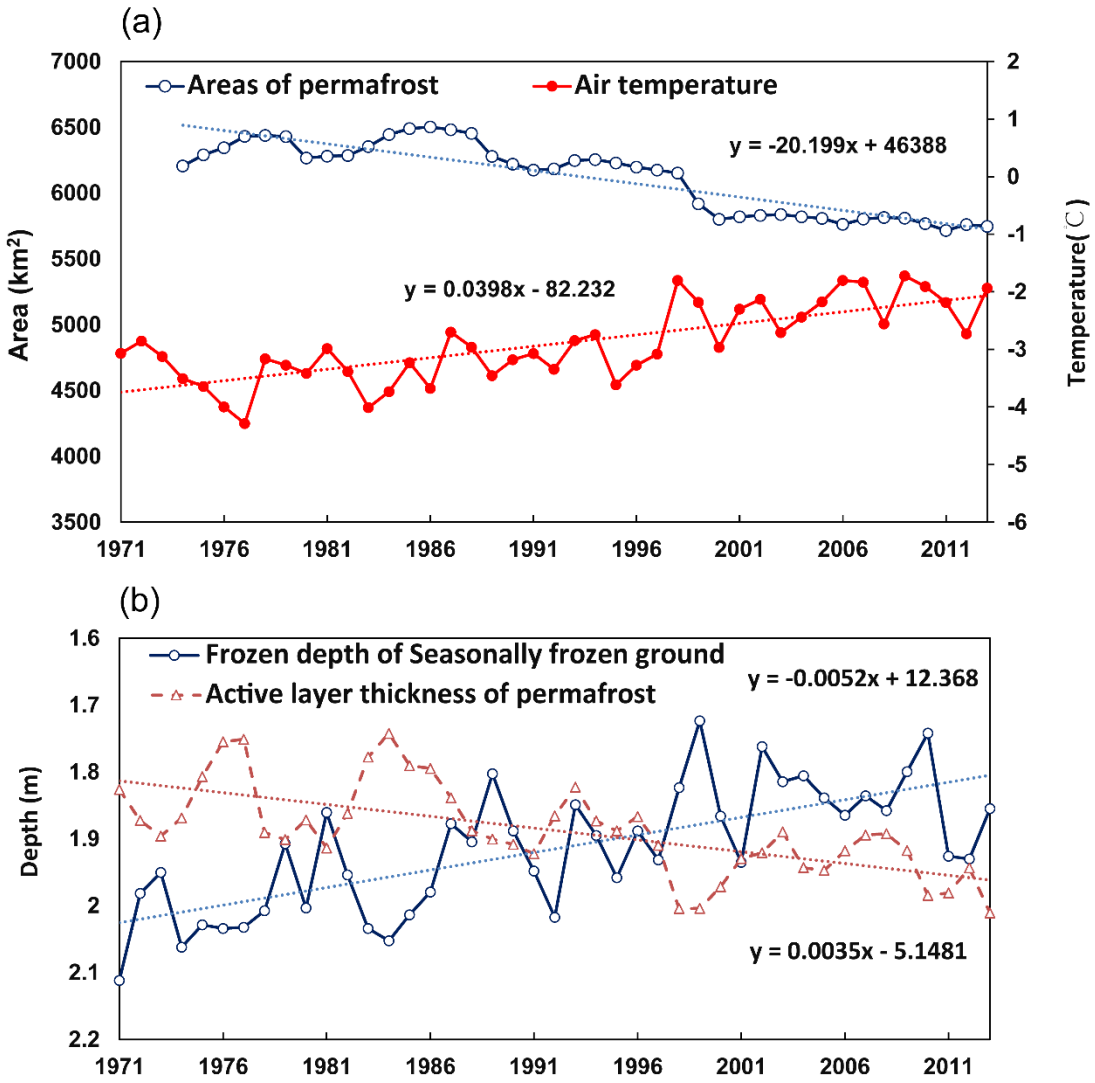

924

925 Figure 10. Change of the frozen soils in the upper Heihe basin: (a) areas of permafrost

926 and basin averaged annual air temperature; (b) the basin averaged annual maximum

927 frozen depth of the seasonally frozen ground and the annual maximum thaw depth of

928 the permafrost

929

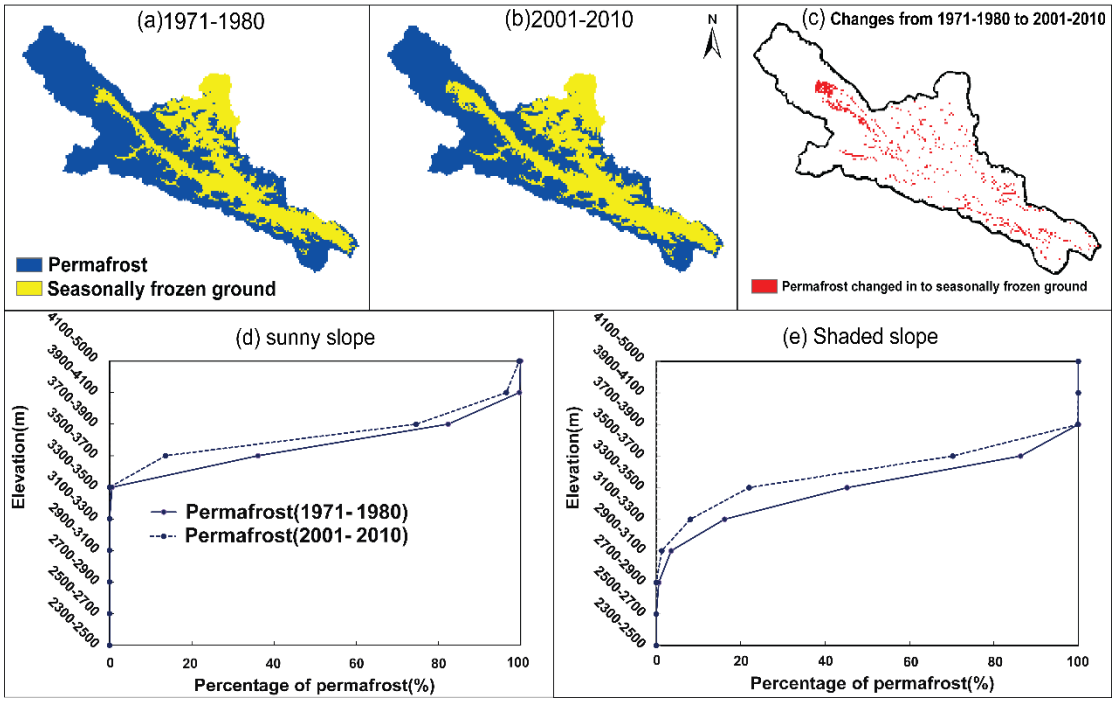

Figure 11. Distribution of permafrost and seasonally frozen ground: (a) distribution in the period of 1971-1980; (b) distribution in the period of 2001-2010; (c) Areas where where permafrost changed into seasonally frozen ground (d) percentage of areas of permafrost on sunny slope; (e) percentage of areas of permafrost on shaded slope (the same legend as (d))

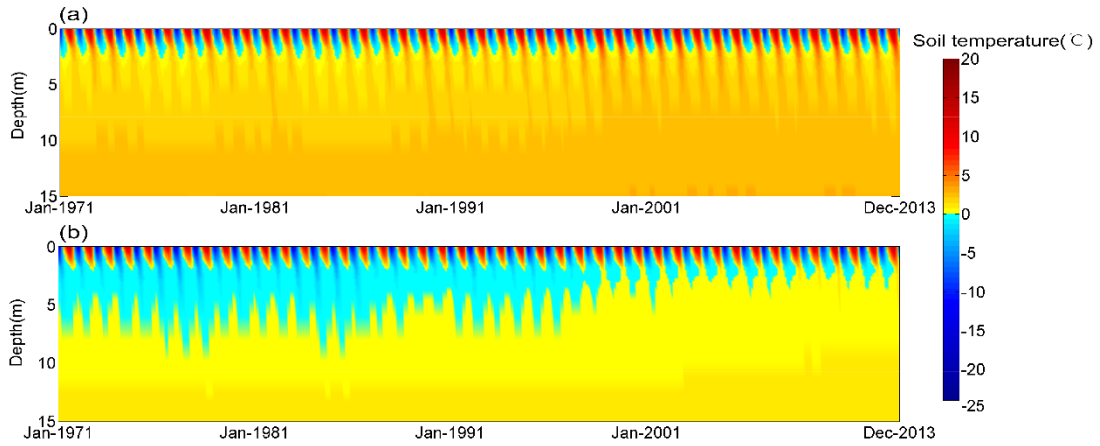

941

942 Figure 12. Spatial averaged monthly soil temperature during the period of 1971-2013

943 in different elevation intervals: (a) the seasonally frozen ground with elevation

944 between 3300-3500 m; (b) the areas where permafrost changed to seasonally frozen

945 ground with elevation between 3500-3700 m

946

947

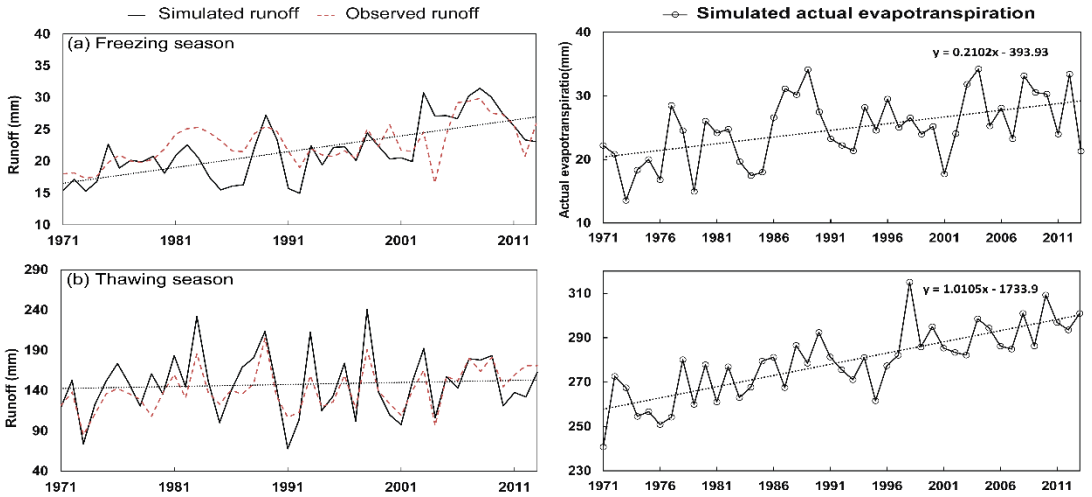

948

949 Figure 13. Changes of the runoff and actual evapotranspiration: (a) in the freezing

950 season; (b) in the thawing season

951

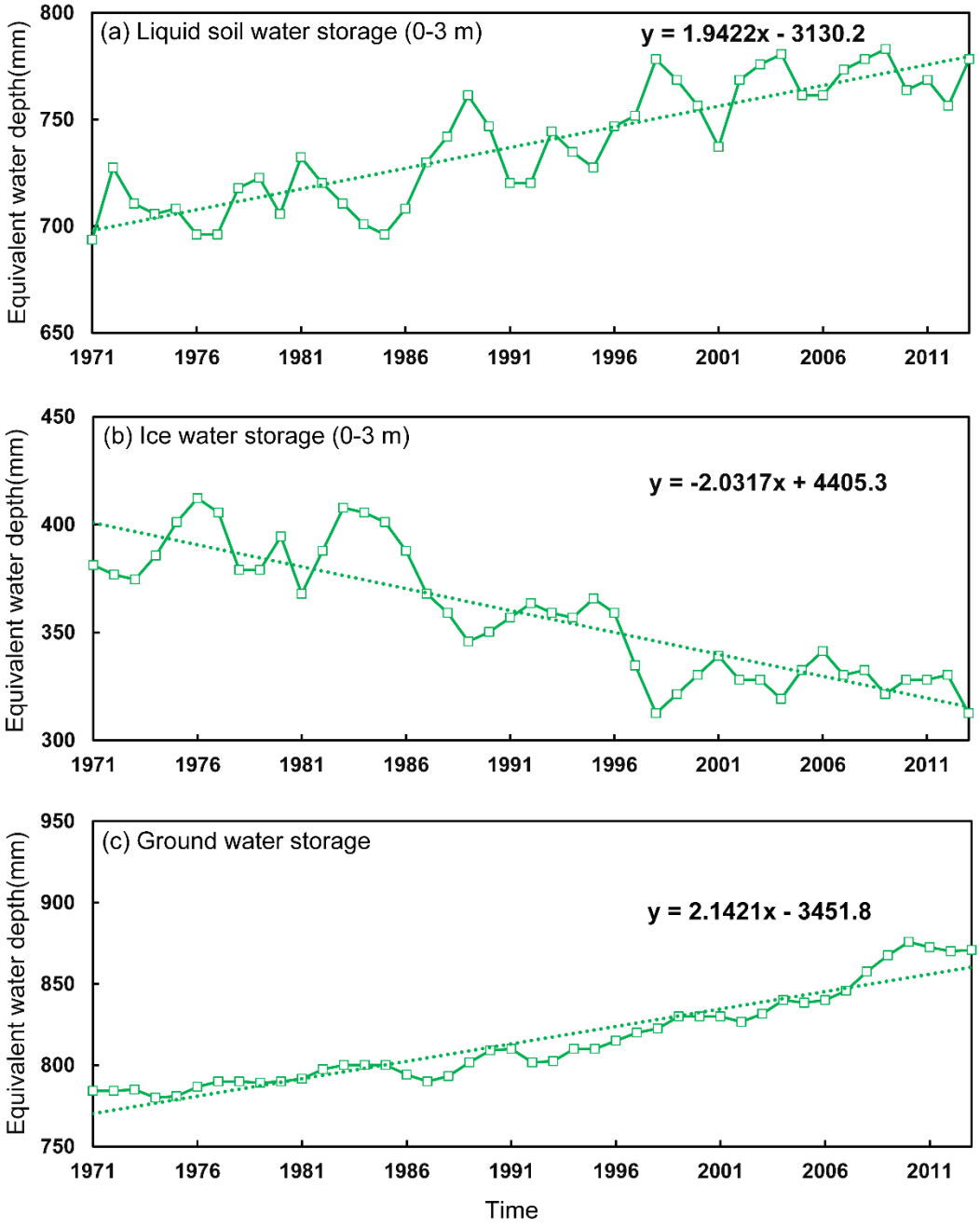

952

953 Figure 14. Changes of the annual water storage (equivalent water depth) during the

954 period of 1971-2013: (a) the liquid soil water storage of the top 0-3 m layer; (b) the ice

955 water storage of the top 0-3 m layer; (c) the groundwater storage

956

957

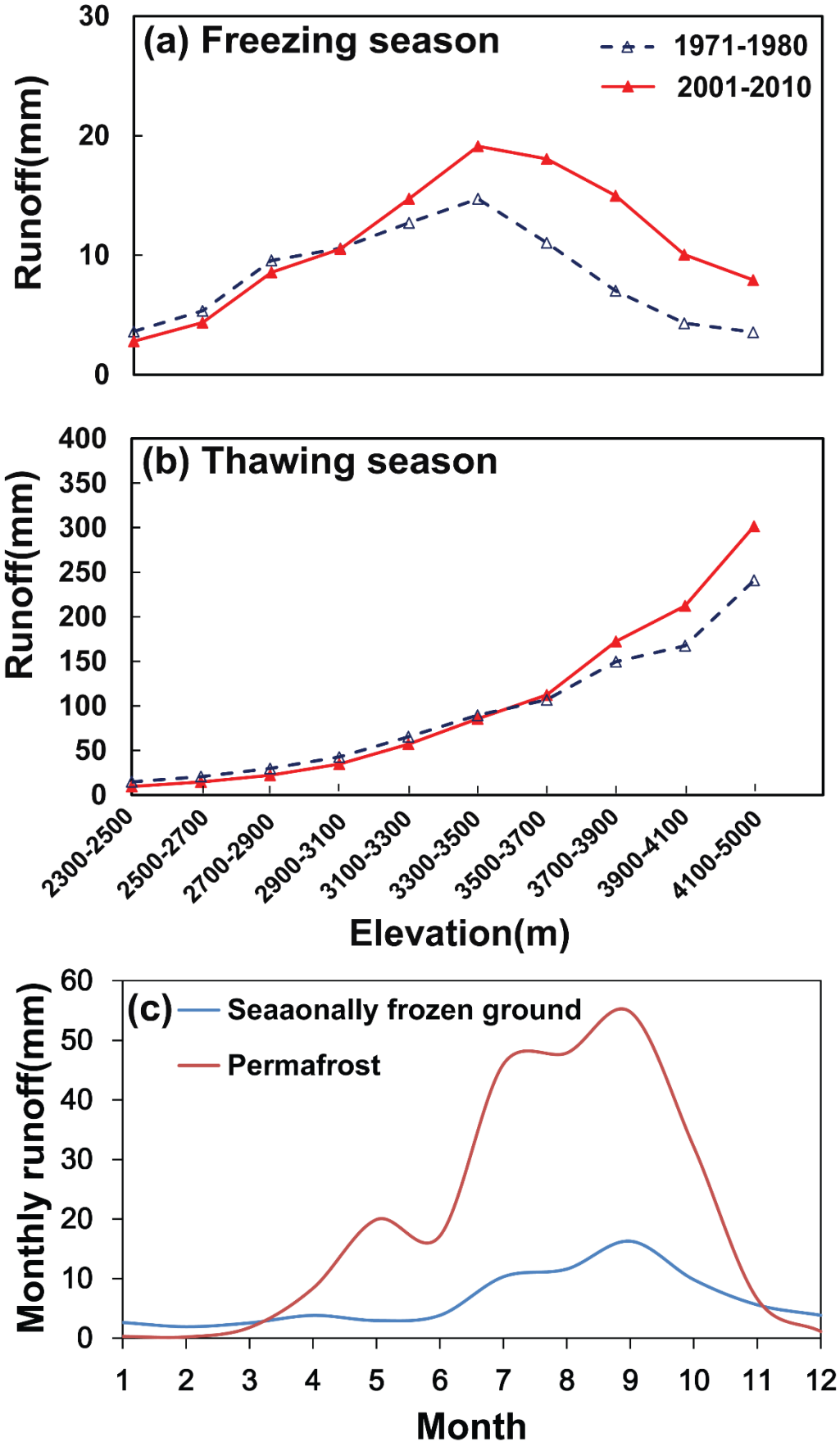
(a) Freezing season
1971-1980
2001-2010
Runoff(mm)
30
20
10
0
(b) Thawing season
Runoff(mm)
400
350
300
250
200
150
100
50
0
2300-2500
2500-2700
2700-2900
2900-3100
3100-3300
3300-3500
3500-3700
3700-3900
3900-4100
4100-5000
Elevation(m)
(c)
Seaaonally frozen ground
Permafrost
Monthly runoff(mm)
60
50
40
30
20
10
0
1
2
3
4
5
6
7
8
9
10
11
12
Month

958

Figure 15. Model simulated runoff change with elevation: (a) in the freezing season, (b) in the thawing season, and (c) seasonal pattern of the runoff in the permafrost areas and in the seasonally frozen ground areas in the period of 2001-2010.

Table list:

Table 1 Major parameters of the GBEHM model

Table 2 Changes in annual basin water balance and runoff components in different seasons

973 Table 1 Major parameters of the GBEHM model

Parameters	Coniferous Forest	Shrub	Steppe	Alpine Meadow	Alpine Sparse Vegetation	Desert
Surface retention capacity (mm)	30.0	25.0	10.0	15.0	15.0	5.0
Surface roughness (Manning coefficient)	0.5	0.3	0.1	0.1	0.1	1.0
Soil reflectance to visible light	0.20	0.20	0.20	0.28	0.14	0.11
Soil reflectance to near-infrared radiation	0.225	0.225	0.225	0.28	0.225	0.225
Leaf reflectance to visible light	0.105	0.105	0.105	0.105	0.105	—
Leaf reflectance to near-infrared radiation	0.35	0.58	0.58	0.58	0.58	—
Leaf transmittance to visible light	0.05	0.07	0.07	0.07	0.07	—
Leaf transmittance to near-infrared radiation	0.10	0.25	0.25	0.25	0.25	—
Maximum Rubsico capacity of top leaf (10^{-5} mol·m^{-2}·s^{-1})	6.0	6.0	3.3	3.3	3.0	—
Plant root depth (m)	2.0	1.0	0.40	0.40	0.1	0.0
Intrinsic quantum efficiency (mol·mol^{-1})	0.08	0.08	0.05	0.05	0.05	—
Canopy top height (m)	9.0	1.9	0.3	0.3	0.2	—
Leaf length (m)	0.055	0.055	0.3	0.3	0.04	—
Leaf width (m)	0.001	0.001	0.005	0.005	0.001	—
Stem area index	0.08	0.08	0.05	0.05	0.08	—

974

975 Table 2 Changes in annual basin water balance and runoff components in different seasons

Decade	Precipitation (mm/yr)	Actual evaporation (mm/yr)	Simulated runoff (mm/yr)	Observed runoff (mm/yr)	Runoff ratio(observed)	Runoff ratio (simulated)	Runoff components (mm/yr)					
							Freezing season (from November to March)			Thawing season(from April to October)		
							T	G	S	T	G	S
1971-1980	439.1	280.8	154.5	143.8	0.33	0.35	18.5	0.0	0.0	136.0	3.5	13.5
1981-1990	492.8	300.0	186.2	174.1	0.35	0.38	20.2	0.0	0.0	166.1	3.1	28.2
1991-2000	471.0	306.1	160.1	157.4	0.33	0.34	20.4	0.0	0.0	139.7	3.8	19.2
2001-2010	504.3	317.4	177.9	174.3	0.35	0.35	27.2	0.0	0.0	150.7	3.7	25.8

976 Note: T means total runoff, G means glacier runoff and S means snowmelt runoff.

977